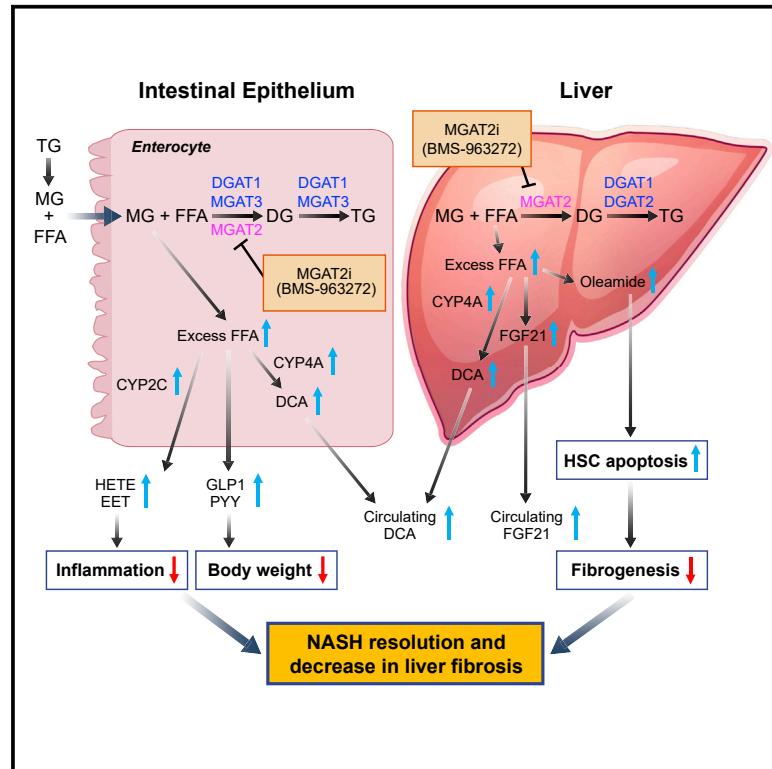# MGAT2 inhibitor decreases liver fibrosis and inflammation in murine NASH models and reduces body weight in human adults with obesity

Graphical abstract

Authors

Dong Cheng, Bradley A. Zinker,
Yi Luo, ..., Edgar D. Charles,
Kimberley A. Lentz, David A. Gordon

Correspondence

dong.cheng@bms.com

In brief

Cheng et al. demonstrate that MGAT2 inhibitor BMS-963272 decreased inflammation and fibrosis in CDAHFD and STAM mice and body weight in human obese subjects, which is consistent with elevation of gut hormone PYY and GLP-1 levels. Long-chain DCAs can serve as a specific translational PD biomarker for MGAT2 inhibitors.

Highlights

- MGAT2 inhibitor BMS-963272 decreased inflammation and fibrosis in murine NASH models

- BMS-963272 increased PYY and FGF-21 and decreased body weight in human subjects

- Elevation of long-chain DCAs is a specific PD biomarker for MGAT2 inhibitors

- MGAT2 inhibition is a promising approach for the treatment of NASH

CellPress

Clinical and Translational Report

MGAT2 inhibitor decreases liver fibrosis and inflammation in murine NASH models and reduces body weight in human adults with obesity

Dong Cheng,[1,10,11,12,]* Bradley A. Zinker,[1,10] Yi Luo,[2,10] Petia Shipkova,[3] Claudia H. De Oliveira,[4] Gopal Krishna,[5] Elizabeth A. Brown,[6] Stephanie L. Boehm,[1] Giridhar S. Tirucherai,[7] Huidong Gu,[2] Zhengping Ma,[1] Ching-Hsuen Chu,[1] Joelle M. Onorato,[3] Lisa M. Kopcho,[8] Ron Ammar,[6] Julia Smith,[1] Pratik Devasthale,[9] R. Michael Lawrence,[9] Steven A. Stryker,[3] Elizabeth A. Dierks,[3] Anthony V. Azzara,[1] Leon Carayannopoulos,[5] Edgar D. Charles,[4] Kimberley A. Lentz,[3] and David A. Gordon[1]

[1]Departments of Discovery Biology Cardiovascular and Fibrosis, Bristol Myers Squibb, Princeton, NJ 08543, USA
[2]Translational Medicine, Bristol Myers Squibb, Lawrenceville, NJ 08543, USA
[3]Pharmaceutical Candidate Optimization, Bristol Myers Squibb, Princeton, NJ 08543, USA
[4]Global Drug Development, Bristol Myers Squibb, Lawrenceville, NJ 08543, USA
[5]ICF Early Clinical Development, Bristol Myers Squibb, Summit, NJ 07901, USA
[6]Translational Bioinformatics, Bristol Myers Squibb, Princeton, NJ 08543, USA
[7]Clinical Pharmacology, Bristol Myers Squibb, Lawrenceville, NJ 08543, USA
[8]Leads Discovery and Optimization, Bristol Myers Squibb, Princeton, NJ 08543, USA
[9]Small Molecule Drug Discovery, Bristol Myers Squibb, Princeton, NJ 08543, USA
[10]These authors contributed equally
[11]Senior author
[12]Lead contact
*Correspondence: dong.cheng@bms.com
https://doi.org/10.1016/j.cmet.2022.10.007

SUMMARY

Monoacylglycerol acyltransferase 2 (MGAT2) is an important enzyme highly expressed in the human small intestine and liver for the regulation of triglyceride absorption and homeostasis. We report that treatment with BMS-963272, a potent and selective MGAT2 inhibitor, decreased inflammation and fibrosis in CDAHFD and STAM, two murine nonalcoholic steatohepatitis (NASH) models. In high-fat-diet-treated cynomolgus monkeys, in contrast to a selective diacylglycerol acyltransferase 1 (DGAT1) inhibitor, BMS-963272 did not cause diarrhea. In a Phase 1 multiple-dose trial of healthy human adults with obesity (NCT04116632), BMS-963272 was safe and well tolerated with no treatment discontinuations due to adverse events. Consistent with the findings in rodent models, BMS-963272 elevated plasma long-chain dicarboxylic acid, indicating robust pharmacodynamic biomarker modulation; increased gut hormones GLP-1 and PYY; and decreased body weight in human subjects. These data suggest MGAT2 inhibition is a promising therapeutic opportunity for NASH, a disease with high unmet medical needs.

INTRODUCTION

Nonalcoholic fatty liver disease (NAFLD) is one of the most common causes of chronic liver disease (Vernon et al., 2011), with increasing prevalence related to high rates of obesity, type 2 diabetes mellitus, insulin resistance, and dyslipidemia. Nonalcoholic steatohepatitis (NASH) is the most severe and progressive form of NAFLD and includes the histologic findings of hepatic steatosis, inflammation, and hepatocyte ballooning degeneration with varying amounts of pericellular fibrosis (Sanyal et al., 2015). The extent of liver fibrosis is the histological feature most closely associated with liver-related outcomes in patients with NASH (Angulo et al., 2015). NASH has been the fastest growing indication leading to liver transplantation in the last 20

years (Adam et al., 2018; Cotter and Charlton, 2020). In Europe, NASH-related cirrhosis accounted for 8.4% of liver transplantations in 2016 compared to 1.2% in 2002 (Adam et al., 2018). In the United States, NASH is the second leading indication for liver transplantation among adults, accounting for 21.5% of liver transplantations performed in 2018 (Cotter and Charlton, 2020). NAFLD/NASH is also considered the fastest growing cause of hepatocellular carcinoma (HCC) in both Europe and the United States (Younossi et al., 2019). In the United States, the incidence of NASH-related HCC is estimated to increase by 137% between 2015 and 2030 (Burra et al., 2020; Estes et al., 2018).

Despite high unmet medical needs, there are no FDA-approved drugs for the treatment of NASH. Diverse targets

including those that mediate glucose, lipid, and bile acid metabolism; inflammation; and fibrosis are currently under study (Konerman et al., 2018; Vernon et al., 2011). As weight loss of 5%–10% has been shown to improve NASH features and increase the chances of NASH resolution (Vilar-Gomez et al., 2015), therapeutic agents that promote weight reduction are a promising approach to treat NASH (Lassailly et al., 2015; Promrat et al., 2010). A primary driver of NAFLD and NASH is the excess accumulation of triglycerides (TGs) in the liver. Increased intake of dietary fats, increased *de novo* lipid synthesis (DNL), and release of free fatty acids (FFAs) by adipose tissue contribute to hepatic TG accumulation (Donnelly et al., 2005). In NAFLD, TGs progressively accumulate in hepatocytes, causing cell ballooning and necroinflammation, which in turn activates hepatic stellate cells (HSCs), leading to fibrosis (Cohen et al., 2011; Tsuchida and Friedman, 2017). Thus, attenuating the influx of TGs to the liver is a potential therapeutic mechanism for NASH (Esler and Bence, 2019). An attractive target to achieve this goal is monoacylglycerol acyltransferase 2 (MGAT2) (Shi and Cheng, 2009; Yang and Nickels, 2015; Yen et al., 2009).

MGAT2 catalyzes the conversion of monoacylglycerol to diacylglycerol. It is highly expressed in the small intestine, where it plays an important role in the resynthesis of TGs during the absorption of dietary fat and assembly in chylomicrons for TG distribution to the liver and peripheral tissues (Cao et al., 2003; Yen and Farese, 2003). Pathologic imbalance in TG homeostasis is a feature of NAFLD and NASH. Increased hepatic MGAT2 expression has been documented in NAFLD; conversely, MGAT2 expression is decreased in patients after gastric bypass surgery, suggesting a role for this enzyme in fatty liver disease (Hall et al., 2012).

In preclinical models, genetic deletion or inhibition of MGAT2 has metabolic benefits. $Mogat2^{-/-}$ mice and high-fat diet (HFD)-induced obese mice treated with an MGAT2 inhibitor showed favorable metabolic changes, such as resistance to HFD-induced weight gain, a delay of TG entry into plasma, a reduction of hepatic TG levels, and an increase in energy expenditure (Take et al., 2016; Yen et al., 2009). Relative to their wildtype (WT) counterparts, $Mogat2^{-/-}$ mice have increased postprandial levels of the metabolically beneficial enteroendocrine hormone glucagon-like peptide-1 (GLP-1) in response to a chronic HFD regimen or a TG bolus (Yen et al., 2009).

BMS-963272, a potent MGAT2 inhibitor, was identified through a *de novo* high-throughput screening and medicinal chemistry campaign (Turdi et al., 2021). In HFD-induced obese mice, BMS-963272 reduced food intake, decreased body weight, and improved insulin sensitivity (Turdi et al., 2021). In the current studies, we evaluated mechanisms of action of BMS-963272 in rodent models and the effects in murine NASH models. The safety, tolerability, and mechanism of action were further assessed in HFD cynomolgus monkeys and healthy human adults with obesity.

RESULTS

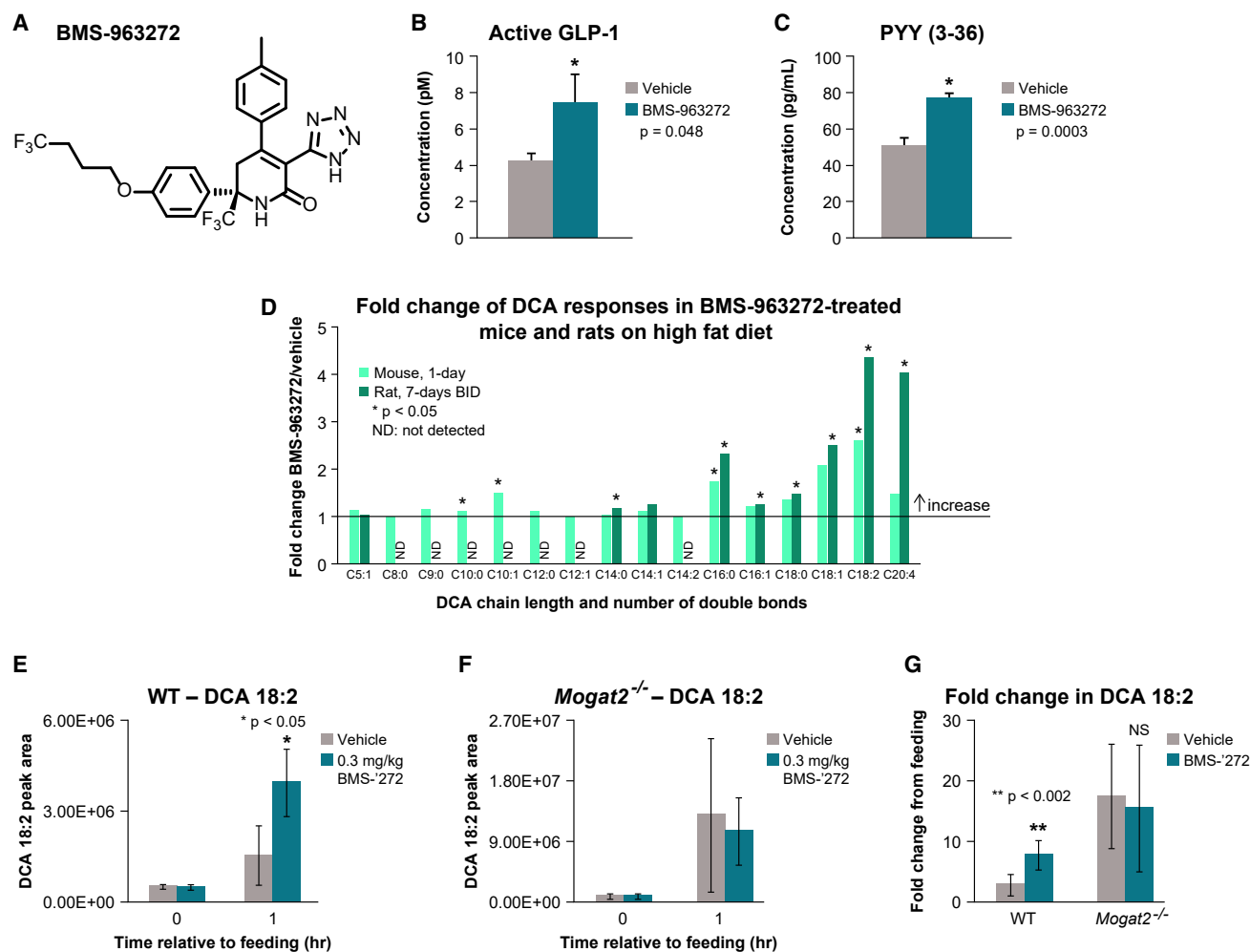### BMS-963272 increased gut hormones and long-chain DCAs

The presence of FFAs in the small intestine stimulates the release of gut hormones and suppresses appetite and energy intake

(Hirasawa et al., 2005; Little et al., 2007). It is hypothesized that MGAT2 inhibition leads to local fatty acid accumulation that promotes enteroendocrine hormone secretion. To explore gut hormone modulation by BMS-963272, a potent and selective MGAT2 inhibitor (Figure 1A) (Turdi et al., 2021), HFD (60% fat from lard) acclimated rats were treated with BMS-963272 for 14 days at 30 mg/kg, p.o., b.i.d. One hour after the last dose of BMS-963272 or vehicle, *ad libitum*-fed animals were sacrificed and plasma was taken for the evaluation of gut hormone levels. As shown in Figures 1B and 1C, active GLP-1 and PYY levels were increased by the BMS-963272 treatment.

To characterize regulation of gene expression in response to MGAT2 inhibition in small intestinal epithelial cells, C57Bl/6J mice were treated with BMS-963272 at 30 mg/kg, p.o., b.i.d., for 7 days under HFD (60% lard fat in diet) conditions. The mRNA of intestinal mucosa was used to conduct an Affymetrix microarray analysis. The most significant upregulations were found in genes related to xenobiotics and fatty acid metabolism, particularly to fatty acid hydroxylation and oxidation. Among them, the expression of *Cyp4a10* was identified as the most highly upregulated by BMS-963272 treatment (Table S1).

The Cyp4A gene family encodes a class of cytochrome P450 enzymes that catalyzes the fatty acid hydroxylation at the ω-position, ultimately leading to the production of dicarboxylic acids (DCAs) (Hardwick, 2008). Using focused metabolomic studies, DCAs with various lengths and double-bond positions were analyzed following BMS-963272 treatment. Methanol extracts of mouse plasma samples (after a 30 mg/kg single dose of BMS-963272 under HFD) and rat plasma samples (after 30 mg/kg b.i.d. dose of BMS-963272 for 7 days under HFD) were subjected to liquid chromatography-mass spectrometry (LC-MS) analyses. As shown in Figure 1D, long-chain DCAs (C-chain length $\geq$ 16) were found to be significantly increased, whereas medium- (C-chain between C8 and C12) and short-chain (C-chain < 8) DCAs were modulated to a much lesser extent. The most consistent and reliable changes were found in DCA 18:1 and 18:2. The preferential increase of long-chain DCAs is consistent with the MGAT2 enzymatic preference for long-chain fatty-acyl Co-As as its substrates (data not shown), suggesting that the observed DCA increase following BMS-963272 treatment might be the result of fatty acid accumulation secondary to MGAT2 inhibition that leads to fatty acid ω-oxidation.

To demonstrate that the BMS-963272-mediated DCA increase is related to MGAT2 activity, $Mogat2^{-/-}$ mice and their WT littermates were trained to consume their 24 h caloric requirement of food within 1 h. After training, these mice were treated with 0.3 mg/kg BMS-963272 (efficacious dose for weight loss in DIO mice; Turdi et al., 2021) or vehicle prior to their 1 h feeding period. As shown in Figure 1E, DCA increased 1 h post-feeding in the vehicle-treated WT mice. This increase was greater in WT mice dosed with BMS-963272. In contrast, in $Mogat2^{-/-}$ mice, BMS-963272 did not alter this response (Figure 1F). Figure 1G shows the DCA 18:2 changes at 1 h post-treatment compared to baseline. In the $Mogat2^{-/-}$ mice, 1 h feeding increased DCA levels to a greater extent as compared to the treatment of BMS-963272 in WT mice. This indicates that genetic deletion, a means to completely eliminate MGAT2 enzyme activity, also increased DCA. Statistical analysis illustrates a

Figure 1. MGAT2 inhibitor BMS-963272 increases gut hormones and long-chain DCAs
(A) BMS-963272 structure.
(B) Increase of active GLP-1.
(C) Increase of PYY (3–36) in HFD-acclimated rats by BMS-963272. n = 8 for both vehicle- and BMS-963272-treated groups. Error bars represent SEM.
(D) Increase of long-chain DCAs in HFD-acclimated rats and mice by BMS-963272. For both rat and mouse studies, n = 10 in vehicle- and BMS-963272-treated groups.
(E–G) DCA (18:2) responses to BMS-963272 in WT and *Mogat2*$^{-/-}$ mice. n = 9 for WT and n = 10 for *Mogat2*$^{-/-}$ mice. Error bars represent SD.
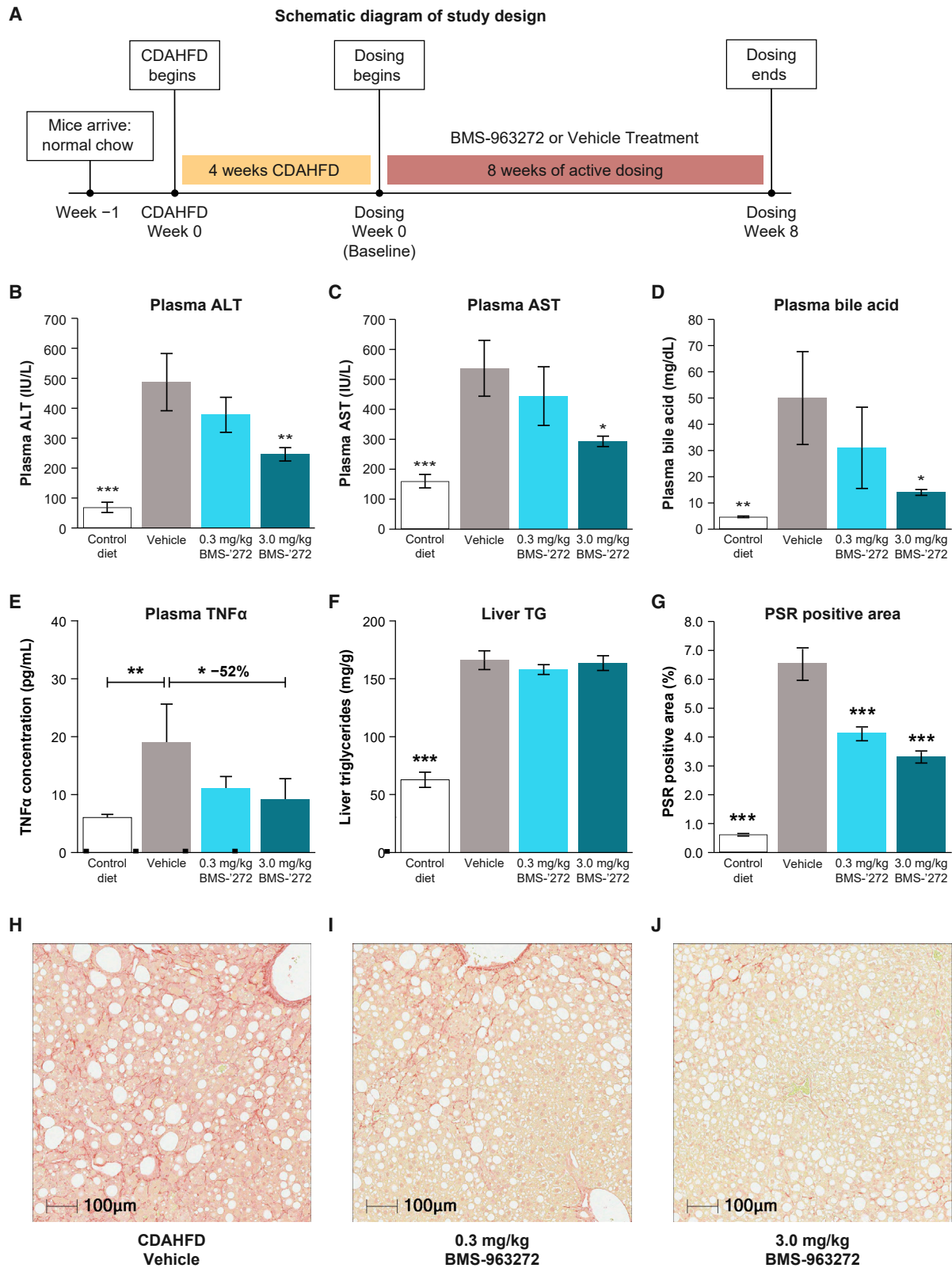
significant elevation in DCA levels produced by BMS-963272 versus vehicle (p < 0.002) in the WT, but no difference between treatment groups in the *Mogat2*$^{-/-}$ mice. These data indicate that BMS-963272-mediated DCA regulation is a result of MGAT2 inhibition.

Therapeutic treatment of BMS-963272 decreases liver fibrosis in CDAHFD murine model of NASH
To test potential effects of the MGAT2 selective inhibitor BMS-963272 in steatosis, inflammation, and fibrosis, a choline-deficient, amino acid-defined, high-fat diet (CDAHFD) murine NASH model was deployed. In this model, the NASH phenotype is induced through the combination of a high-fat (60% kcal from fat) and methionine-/choline-deficiency diet (Matsumoto et al., 2013). As shown schematically in Figure 2A, C57BL/6J mice were provided a CDAHFD for 4 weeks, which generated an early

NASH phenotype. Then these mice were therapeutically dosed orally once daily for 8 weeks with either 0.3 or 3.0 mg/kg BMS-963272 or vehicle for a total of 12 weeks on diet. Body weight and food intake were measured over the course of the 8-week treatment period. Mice were sacrificed 2 h after their final dose of vehicle or compound, in the postprandial state, and plasma and liver were harvested for analyses.

BMS-963272 did not change food intake, body weight, liver weight, and liver/body weight ratio. BMS-963272 decreased alanine transaminase (ALT) and aspartate aminotransferase (AST), markers of hepatic injury, in a dose-dependent manner (Figures 2B and 2C). Plasma ALT levels were 68.9 ± 17.3, 486.5 ± 95.5, 378.0 ± 8.5, and 246.1 ± 22.2 IU/L for control diet, CDAHFD vehicle, 0.3 mg/kg, and 3.0 mg/kg BMS-963272 groups, respectively (p < 0.001 and p < 0.01 for control diet and 3.0 mg/kg BMS-963272 versus CDAHFD vehicle). Plasma

A Schematic diagram of study design

B Plasma ALT

C Plasma AST

D Plasma bile acid

E Plasma TNFα

F Liver TG

G PSR positive area

H CDAHFD Vehicle

I 0.3 mg/kg BMS-963272

J 3.0 mg/kg BMS-963272

(legend on next page)

AST levels were 159.6 ± 22.4, 537.0 ± 93.3, 443.7 ± 97.9, and 292.9 ± 17.5 IU/L for control diet, CDAHFD vehicle, 0.3 mg/kg, and 3.0 mg/kg BMS-963272 groups, respectively (p < 0.001 and p < 0.05 for control diet and 3 mg/kg BMS-963272 versus CDAHFD vehicle, respectively) (Figures 2B and 2C).

In the CDAHFD model, the bile acid metabolic enzymes and transporters are significantly altered, resulting in increased bile acid efflux from hepatocytes into plasma rather than bile (Suga et al., 2019). BMS-963272 reversed the CDAHFD-mediated increase of plasma bile acid levels. The plasma bile acid levels were 4.7 ± 0.3, 49.4 ± 17.7, 30.6 ± 15.5, and 14.0 ± 1.1 IU/L for control diet, CDAHFD vehicle, 0.3 mg/kg, and 3 mg/kg BMS-963272 groups, respectively (p < 0.01 and p < 0.05 for control diet and 3.0 mg/kg BMS-963272 versus CDAHFD, respectively) (Figure 2D).

The CDAHFD diet significantly elevated plasma tumor necrosis factor alpha (TNFα), a marker of inflammation, by approximately 4-fold as compared to control diet. BMS-963272 reversed CDAHFD-mediated elevation of TNFα levels. At 3.0 mg/kg, BMS-963272 significantly decreased TNFα by 52% (p < 0.05) (Figure 2E).

The CDAHFD diet significantly elevated liver TGs compared to control diet (liver TG levels: control diet, 62.8 ± 6.6 mg/g; CDAHFD vehicle, 166.2 ± 8.1 mg/g; p < 0.01) and BMS-963272 did not change the elevated TG levels (Figure 2F).

The effect of BMS-963272 on liver fibrosis was determined by the measurement of picrosirius red (PSR) stain. The PSR-positive area was significantly reduced by both 0.3 mg/kg BMS-963272 (−40% to normalization versus CDAHFD vehicle, p < 0.001) and 3.0 mg/kg BMS-963272 (−54% to normalization versus CDAHFD vehicle, p < 0.001), indicating a significant reduction in liver fibrosis (Figure 2G). Representative PSR images are shown in Figures 2H–2J. Abundant and intense pink PSR stains were evident in the liver of CDAHFD vehicle-treated mice. The intensity of the pink PSR stains was visibly attenuated in the liver of CDAHFD mice treated with both 0.3 mg/kg and 3 mg/kg BMS-963272 (Figures 2H–2J).

Global regulation of inflammation and fibrosis pathways by BMS-963272 in the liver and small intestine in CDAHFD mice

To analyze the gene expression profile for the whole genome in the CDAHFD mice, we applied RNA sequencing (RNA-seq) technology to analyze the liver and jejunum tissues where *Mogat2* is highly expressed. Using the criteria of p ≤ 0.1 after adjusting for multiple testing, 4,413 genes in liver and 4,143 genes in jejunum were regulated by 3.0 mg/kg BMS-963272 relative to the vehicle control. Absolute logFC cutoffs of log2(1.15) and log2(1.2), respectively, were applied to more stringently define the liver- and jejunum-regulated genes and assess pathways for enrichment of gene regulation. Among the top 25 most highly enriched pathways in the liver, strong downregulation was observed

for pathways related to fibrosis (TGFβ- and integrin-related signaling), cell adhesion, extracellular matrix, and the epithelial-to-mesenchymal transition (EMT), which include many downregulated collagen genes (Figure 3A; Table S2). Inflammation and oxidative stress pathways were also downregulated (Figure 3A; Table S2). Although no enriched pathways were predominantly upregulated, *Fgf21* was among the strongest upregulated gene in the liver with approximately 3-fold increase in 3.0 mg/kg BMS-963272-treated mice compared to vehicle (Table S2).

The most highly upregulated pathways in jejunum included genes involved in fatty acid β-oxidation and ω-oxidation and xenobiotic metabolism (Figure 3B; Table S3). The most highly upregulated gene was *Cyp4a10* by 3.54-fold (p = 2.6×10^{-19}) (Table S3), consistent with the finding in HFD-induced obese mice (Table S1). In addition, the most highly downregulated pathways in jejunum included immune-related pathways, particularly those related to T cell generation and Th17 cytokines (Figure 3B; Table S3).

Intestinal HETE and EET increased by BMS-963272 treatment in CDAHFD mice

Among the top upregulated enzymes involved in xenobiotic metabolism in jejunum, the expression of *Cyp2c29* and *Cyp2c65* was increased by 1.57-fold (p = 0.06) and 1.36-fold (p = 2.6×10^{-11}), respectively (Table S3). These cytochrome P450 enzymes are known to have arachidonic epoxygenase activity for the synthesis of hydroxyeicosatetraenoic acid (HETE) and epoxyeicosatrienoic acid (EET) molecules that are reported to mediate inflammation-resolving pathways (Luo et al., 1998; Serhan et al., 2008). LC-MS analysis of extracts from the small intestine of CDAHFD mice revealed that treatment with 3.0 mg/kg BMS-963272 increased the levels of 5-HETE, 8-HETE, 12-HETE, 15-HETE, and 5,6-EET compared to vehicle control (Figures 4A, 4B, and 4D–4F). Treatment with both 0.3 mg/kg and 3.0 mg/kg BMS-963272 did not change 11-HETE levels (Figure 4C).

Prophylactic treatment of STAM mice by BMS-963272 improves NAFLD activity score and liver fibrosis
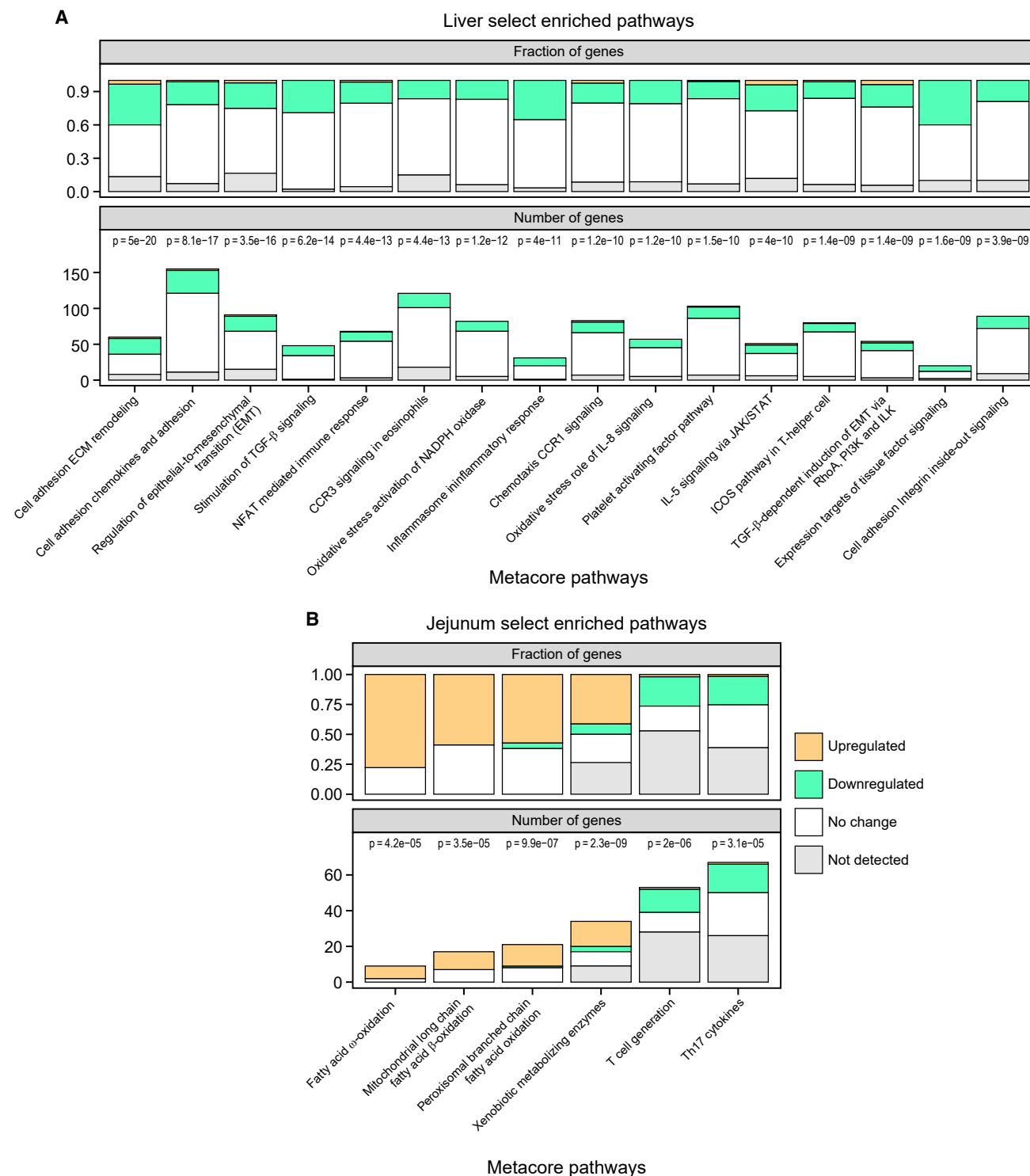
To further investigate the effect of BMS-963272 in steatosis, inflammation, and liver fibrosis, we conducted a prophylactic treatment study in STAM NAFLD/NASH model. Starting at 6 weeks of age, 8 NASH mice/group were orally administered prophylactically either vehicle or BMS-963272 at 0.3 or 3.0 mg/kg for 3 weeks. At 9 weeks of age, plasma and liver samples were analyzed. There were no significant changes in mean body weight, liver weight, liver/body weight ratio, plasma ALT, plasma glucose, plasma and liver TG, and cholesterol levels between the vehicle group and BMS-963272 treatment groups. Histological analyses revealed that there were inconsistent reductions of composite NAFLD activity score (NAS) in both

---

Figure 2. Therapeutic treatment of BMS-963272 decreases liver fibrosis in CDAHFD murine model of NASH

(A) Schematic diagram of study design.

(B–G) Treatment effects by BMS-963272 in CDAHFD. (B) Plasma ALT, (C) plasma AST, (D) plasma bile acid, (E) plasma TNFα, (F) liver TG, and (G) liver histological PSR-positive area. n = 10 for all groups. Error bars represent SEM.

(H–J) Representative PSR-stained histology images. (H) CDAHFD vehicle, (I) 0.3 mg/kg BMS-963272-treated CDAHFD liver, and (J) 3.0 mg/kg BMS-963272-treated CDAHFD liver.

Figure 3. Decreases in inflammation and fibrosis pathways by BMS-963272 in CDAHFD mice
(A) Liver select enriched pathways.
(B) Jejunum select enriched pathways impacted by BMS-963272 in CDAHFD mice.

BMS-963272 0.3 and 3.0 mg/kg groups compared with vehicle group (Figure 5A). The average NAS scores were 5.1 ± 0.4, 4.4 ± 1.2, and 4.0 ± 0.9 for vehicle, 0.3 mg/kg, and 3.0 mg/kg

BMS-963272 groups, respectively. There were 1 or 2 mice out of 8 mice that differed from the vehicle controls in lobular inflammation and hepatocyte ballooning scores; however,
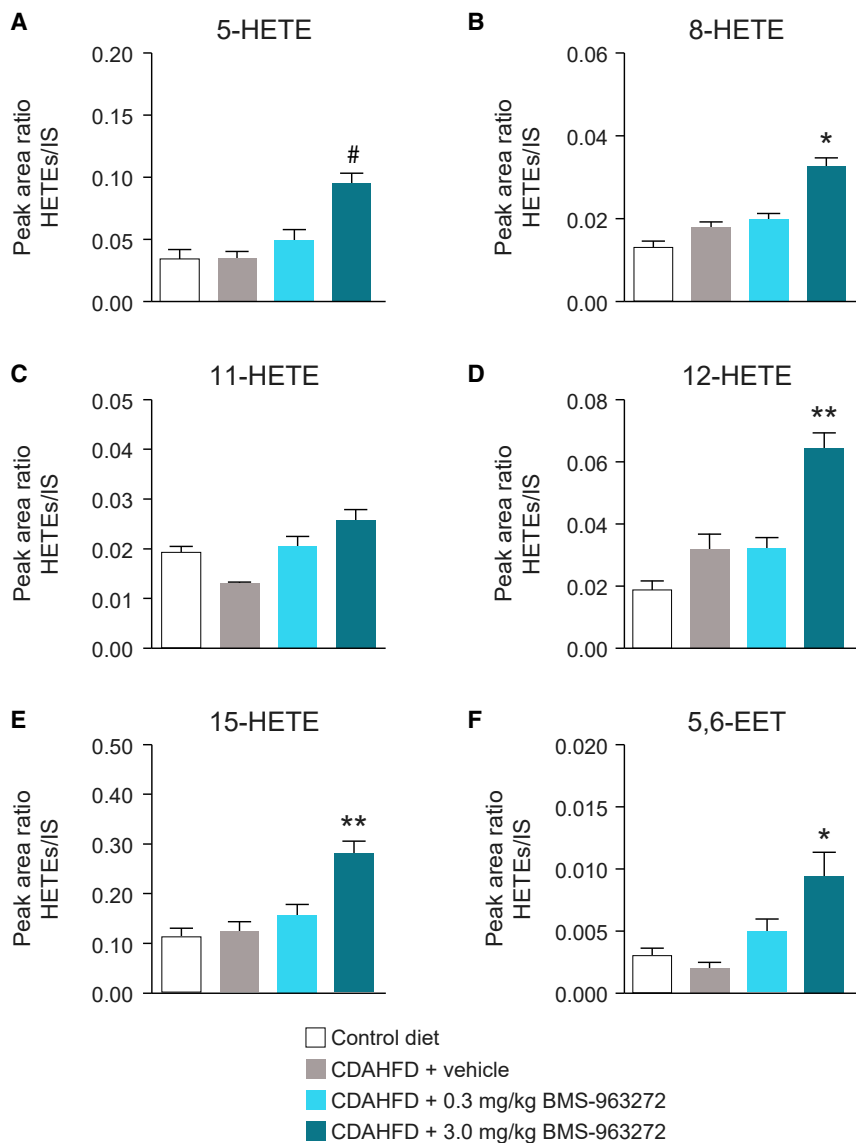
Figure 4. Effect of intestinal HETE and EET levels by BMS-963272 in CDAHFD mice

Regulation of intestinal (A) 5-HETE, (B) 8-HETE, (C) 11-HETE, (D) 12-HETE, (E) 15-HETE, and (F) 5,6-EET by BMS-963272. #p = 0.07, *p < 0.05, **p < 0.01. n = 10 for all groups. Error bars represent SD.

(Figure 1D), the most prominent increases of DCA responding to treatment with BMS-963272 in the STAM mice were the long-chain DCAs. C18:1, C18:2, and C20:4 DCAs were increased following treatment with 0.3 mg/kg BMS-963272 by 9-fold, 2-fold, and 9-fold and with 3.0 mg/kg BMS-963272 by 12-fold, 3-fold, and 12-fold, respectively (all p < 0.05).

The metabolomic profiling of liver samples revealed BMS-963272 caused relatively moderate increases in liver DCAs (Figure 5E). In contrast to the plasma results, 18:2 DCA was decreased by BMS-963272-treatment and 20:4 DCA was not measurable. The most prominent DCA increase responding to BMS-963272 was 18:1 DCA, which was increased 4.7-fold and 6.8-fold following treatment with 0.3 mg/kg and 3.0 mg/kg BMS-963272, respectively (both p < 0.05) (Figure 5E). In the liver tissue samples, BMS-963272 also caused significant but non-dose-proportional increases in liver fatty acid amides (Figure 5F). The most abundant fatty acid amide in the liver of STAM mice was oleamide, which was followed by palmitamide, linoleamide, stearamide, and palmitolamide. Compared to vehicle, oleamide, palmitamide, linoleamide, stearamide, and palmitolamide were increased 11-fold, 13-fold, 14-fold, 13-fold, and 14-fold by 0.3 mg/kg BMS-963272 (all p < 0.05) and 8-fold, 9-fold, 9-fold, 9-fold, and 9-fold by 3.0 mg/kg BMS-963272 (p < 0.05 for palmitamide and stearamide) (Figure 5F).

Oleamide is an endocannabinoid molecule (De Petrocellis et al., 2000), and it was reported that treatment with endocannabinoid 2-arachidonoylglycerol (2-AG) and methanandamide, a stable analog of endocannabinoid anandamide, caused apoptosis of activated human HSCs, the progenitors of hepatic fibrogenic myofibroblasts (Julien et al., 2005). To test whether oleamide exerts similar effects, human primary HSCs, activated by culturing on the stiff surface of plastic plates that confers upon the HSCs a myofibroblast phenotype, were treated with oleamide along with other cannabinoids arachidonylethanolamine (AEA, or anandamide), di-homo-gamma-linolenoyl ethanolamide (DHLEA), docosahexanoyl ethanolamide (DHEA), and 2-AG as controls. Similar to AEA, DHLEA, DHEA, and oleamide caused cell death of activated human HSCs at 10 and 100 μM but not at 1 μM. 2-AG caused cell death at 100 μM, but not at
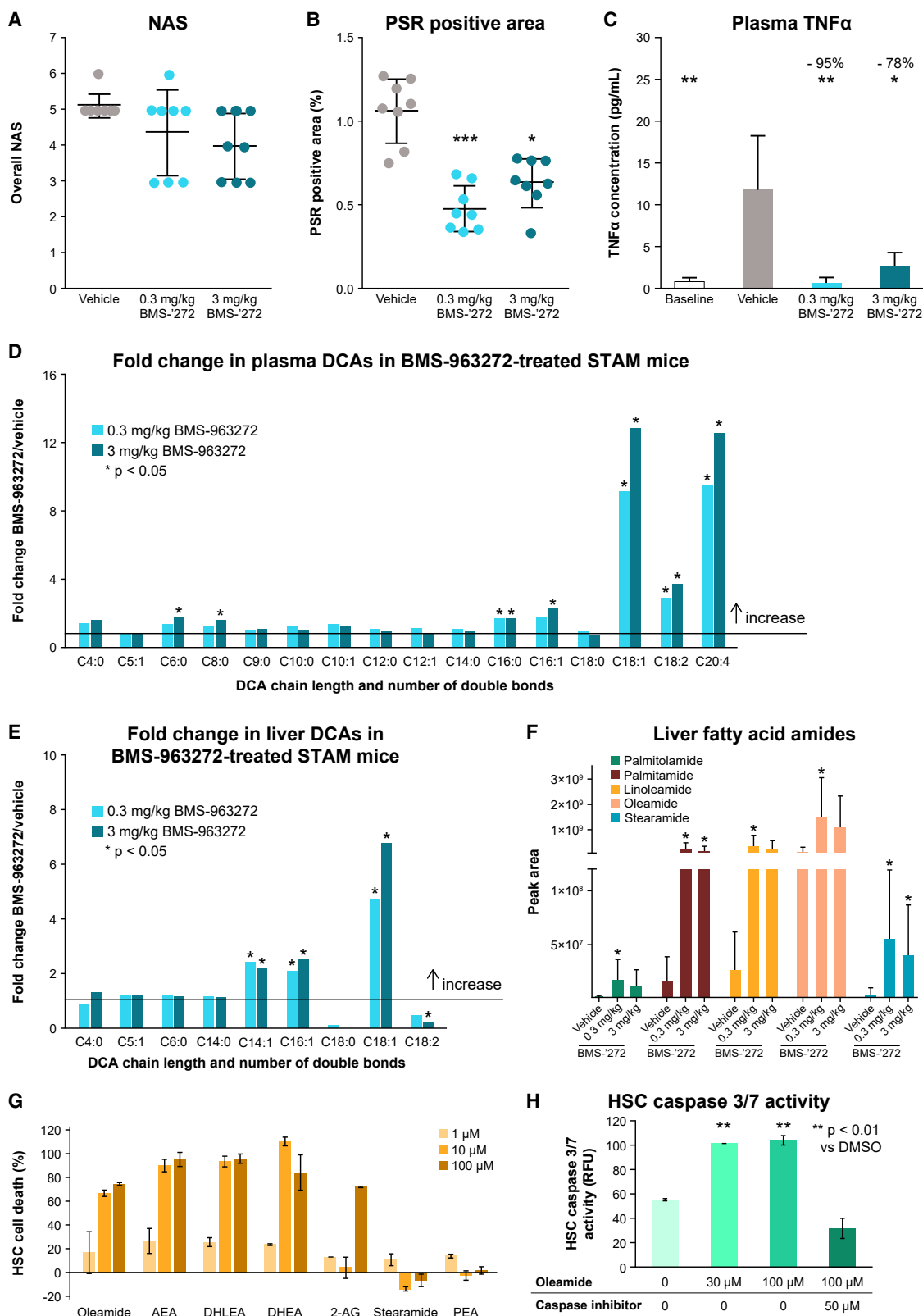
steatosis remained stable (Table S4). BMS-963272 significantly decreased the fibrosis area at both 0.3 and 3.0 mg/kg compared to vehicle group as shown by PSR staining (Figure 5B). PSR-positive areas (%) were 1.07 ± 0.19, 0.49 ± 0.13, and 0.64 ± 0.15 for vehicle, 0.3 mg/kg, and 3.0 mg/kg BMS-963272, respectively (p < 0.0001 for 0.3 mg/kg BMS-963272 and p < 0.01 for 3 mg/kg BMS-963272 versus vehicle).

To investigate the inflammatory state of the BMS-963272-treated STAM mice, plasma TNFα levels were measured. The vehicle-treated group at 9 weeks of age had significantly elevated TNFα levels by approximately 10-fold from baseline at 6 weeks. Treatment with 0.3 mg/kg and 3.0 mg/kg BMS-963272 decreased TNFα significantly by 95% and 78%, respectively (p < 0.05 for both) (Figure 5C).

Plasma and liver samples collected at 9 weeks were also subjected to LC-MS metabolomic profiling. The most notable changes were increases in the plasma DCA levels (Figure 5D). Consistent with the findings in the HFD-treated rats and mice

CellPress

Figure 5. Prophylactic treatment of STAM mice by BMS-963272 improves NAFLD activity score and liver fibrosis

(A–C) Prophylactic treatment of STAM mice by BMS-963272 decreases (n = 8 for all groups) (A) liver histological NAFLD activity score (NAS), (B) liver histological PSR-stained positive area, and (C) plasma TNFα levels.

1 and 10 μM, suggesting that oleamide might be more potent than 2-AG in mediating the cell death effect for the activated HSCs (Figure 5G). In addition, stearamide, an oleamide analog with no double bond in the fatty acid chain, and palmitoyl ethanolamide (PEA), an AEA analog without double bond in the fatty acid moiety, were also tested. Neither stearamide nor PEA caused HSC cell death (Figure 5G), suggesting that double bond(s) in the fatty acid moiety of cannabinoids are important for the cell death effect for HSCs. The lack of activity of these closely related fatty acid amides serves as a control for non-specific fatty acid toxicity from oleamide. One of the hallmarks of apoptosis is its dependence on caspase 3/7 activation (Slee et al., 1999; Thornberry et al., 1997). To test if the oleamide-mediated HSC cell death is apoptotic, caspase 3/7 activity was measured. Indeed, oleamide treatment elevated caspase 3/7 activity, which was reversed by treatment with caspase 3/7 inhibitor (Z-VAD-FMK; Figure 5H). We also tested the effect of DCA16:0 and DCA18:1 on HSCs. Neither DCA16:0 nor DCA18:1 caused an apoptotic effect on the activated HSCs (data not shown).

To assess if BMS-963272 caused fewer HSCs in STAM mice, we conducted immunohistochemical staining of liver tissues by anti-α-SMA antibody (Abcam, USA) and quantified α-SMA-positive areas. Treatment of 0.3 and 3 mpk BMS-963272 caused a trend of decrease in α-SMA-positive areas compared with vehicle, but did not meet statistical significance (data not shown).

Absence of diarrhea in HFD-fed cynomolgus monkeys following treatment with BMS-963272

Clinical gastrointestinal (GI) effects, most notably diarrhea, led to the discontinuation of development of several DGAT1 inhibitors (Denison et al., 2014; DeVita and Pinto, 2013). To develop a preclinical model susceptible to DGAT1-induced diarrhea, cynomolgus monkeys were fed an HFD (24% of kcal from fat). After establishing background diarrhea incidence using both normal chow and HFD, 12 monkeys (6/sex) were administered test compounds for 4 days. Two monkeys/sex served as vehicle controls. After a 10-day washout period, the dose was escalated and the same animals dosed for another 4-day period. The process was repeated until definitive evidence of diarrhea was observed. DGAT1-selective inhibitor PF-04620110 (Figure S1) (Dow et al., 2011) was evaluated at 0.1, 0.3, and 1 mg/kg/day in monkeys fed an HFD, and caused diarrhea at ≥0.3 mg/kg/day within 4 days, at plasma concentrations comparable to those that caused diarrhea in human clinical trials (Maciejewski et al., 2013). After a 1.5-month washout period, BMS-963272 was tested using the same monkeys and dosing paradigm. Doses of 1 and 10 mg/kg/day did not cause diarrhea/unformed feces within 4 days (Figure 6A).

To test the acute effects of BMS-963272 on TG absorption in cynomolgus monkeys, an oral lipid tolerance test (oLTT) was conducted using eleven monkeys (5 males, 6 females) that had been acclimated to an HFD (Test Diet 5TNU primate diet,

46.9% of kcal from fat). The monkeys were food-deprived overnight and were then dosed p.o. with 1 mg/kg BMS-963272 or vehicle. One hour later, a p.o. bolus of intralipid (7 mL/kg intralipid 20%, a 20% soybean oil emulsion) was administered. Two weeks after the initial dosing, all monkeys were retested in a within-subject crossover design, allowing each animal to serve as its own control. As shown in Figure 6B, treatment with BMS-963272 did not cause significant changes in plasma TG levels at any time point, relative to vehicle treatment. DCA 18:2 in the plasma from the cynomolgus monkey oLTT experiment was also measured. As shown in Figures 6C and 6D, treatment with BMS-963272 produced increases in DCA 18:2 in both male (n = 5) and female (n = 6) cynomolgus monkeys. However, given the variable nature of the responses, this effect failed to reach statistical significance.

Pharmacokinetics of BMS-986272 in healthy human adults with obesity

The pharmacokinetics (PK), safety, and tolerability of BMS-963272 were assessed in two Phase 1 studies in healthy human adults with obesity. BMS-963272 demonstrated acceptable safety and tolerability at daily doses up to 300 mg (QD, p.o. for 14 days) in a Phase 1 multiple ascending dosing (MAD) study (NCT02327273). However, due to a relatively short half-life (T-half ∼3 h), optimal daily exposure was not attained with once-daily dosing. Nevertheless, BMS-963272 demonstrated biomarker modulation by increasing postprandial DCA levels during an oLTT performed at the maximum concentration (C_{max}) corresponding to 1 h post-BMS-963272 dosing (data not shown).

A second Phase 1 study in healthy human adults with obesity was conducted to investigate the PK, pharmacodynamics (PD), and safety and tolerability of BMS-963272 with multiple daily oral dosing for 14 days (300 mg once daily [Q24H], 300 mg every 12 h [Q12H], or 300 mg every 8 h [Q8H]) (NCT04116632). Adults ≥ 18 years to ≤60 years, with a body mass index (BMI) of ≥30 to ≤40 kg/m², excluding women of child-bearing potential, in good general health were eligible for the study (additional inclusion and exclusion criteria are presented in the clinical study protocol section of STAR Methods). A total of 36 participants were randomized, with 12 participants per group within each dose group; the participants were randomized to receive BMS-963272 (n = 8) or a matching placebo (n = 4). Overall, 35 participants received all scheduled study treatments and completed the study, with 1 participant (BMS-963272 300 mg Q24H) discontinuing the study after 6 doses due to poor venous access. The CONSORT diagram of the trial is described in Figure S2. Baseline demographic characteristics are described in Table S5.

Mean (±SD) trough plasma concentration (C_{trough}) time profiles for BMS-963272 were assessed from day 1 through day 14 and are presented in Figure 7A. No accumulation of plasma BMS-963272 was apparent following multiple doses, which is consistent with the observed short half-life. Steady state was reached by day 2 of administration for all dose groups, based on the

---

(D–F) Treatment of STAM mice by BMS-963272 increases (D) plasma long-chain DCAs, (E) liver tissue long-chain DCAs, and (F) liver tissue fatty amides.
(G) Oleamide treatment causes HSC cell death *in vitro*.
(H) Treatment of HSCs by oleamide increases caspase 3/7 activity.
Error bars in (A), (B), and (F) represent SD and in (C), (G), and (H) represent SEM.
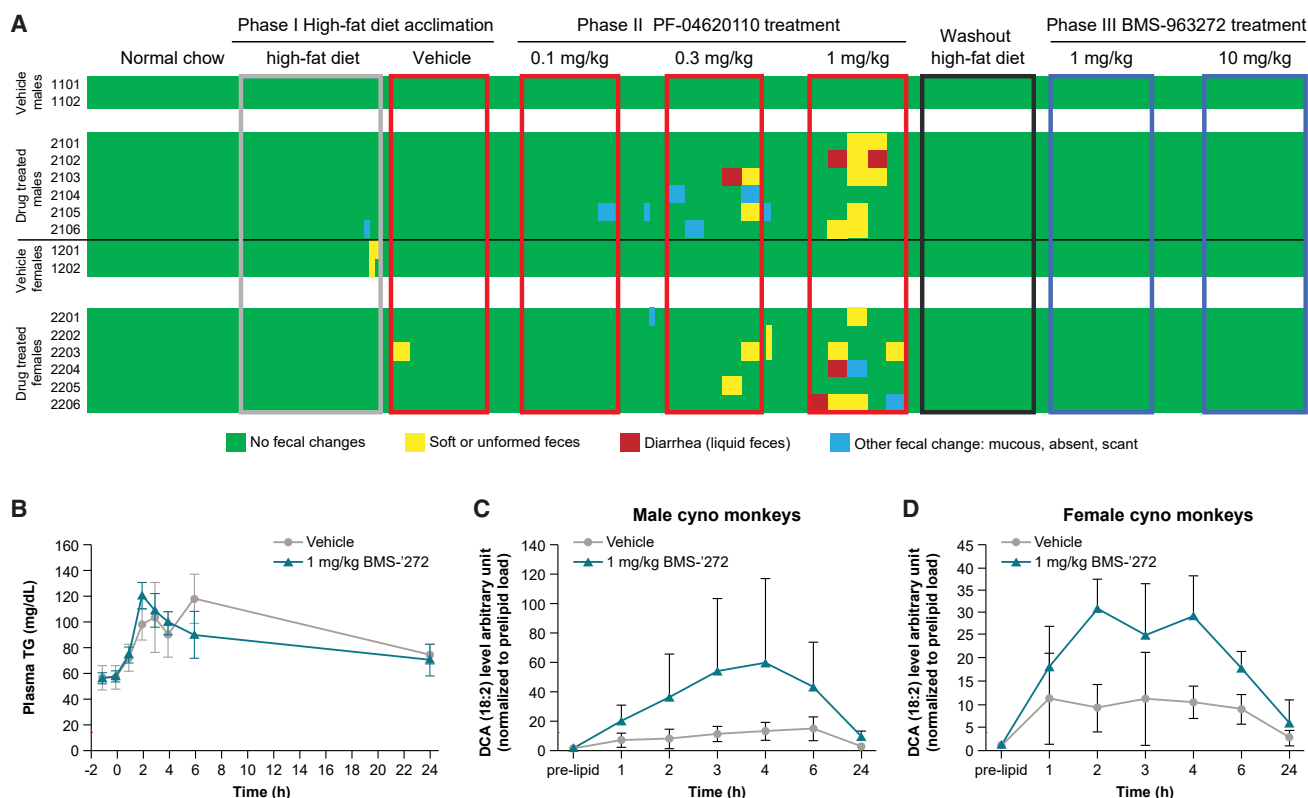
Figure 6. Absence of diarrhea in HFD-fed cynomolgus monkeys following treatment with BMS-963272

(A) Diarrhea log of HFD-fed cynomolgus monkeys. Gray box, 1-month HFD acclimation; red box, treatment with vehicle or PF-04620110, 4 days per dose; black box, 1.5-month washout under HFD; blue box, treatment with BMS-963272, 4 days per dose.

(B) TG excursion time course in HFD-fed cynomolgus monkeys in oLTT. Total, n = 11: 5 males, 6 females. Error bars represent SD.

(C and D) DCA responses in HFD-fed cynomolgus monkeys in oLTT. (C) Males and (D) females. Total, n = 11: 5 males, 6 females. Error bars represent SD.

similarity in mean trough plasma concentrations on day 2 through day 14. Mean plasma trough concentrations increased with more frequent dose administration: geometric mean (±SD) was 6.72 ng/mL (±3.23 ng/mL), 39.0 ng/mL (±22.4 ng/mL), and 91.3 ng/mL (±91.8 ng/mL) for Q24H, Q12H, and Q8H dosing groups, respectively.

Tolerability of BMS-963272 in adults with obesity

BMS-963272 was generally safe and well tolerated in this study, with no reported serious adverse events (SAEs). There were no changes in the number of daily bowel movements observed. The most frequent treatment-emergent adverse event (TEAE) was diarrhea, which was observed in 1 subject receiving 300 mg QD BMS-963272, 2 participants receiving 300 mg Q12H, and 3 receiving 300 mg Q8H. All diarrhea TEAEs were mild, except for 1 moderate event. These incidences did not lead to any treatment discontinuation. This is in distinct contrast to the report by Denison et al. that 11/18 subjects treated with DGAT1 inhibitor AZD7687 withdrew from the study due to GI intolerance (Denison et al., 2014).

Pharmacodynamic effects of BMS-986272 in healthy adults with obesity

To assess the PD biomarker effects of BMS-963272, each participant was administered an oLTT consisting of a high-fat

liquid meal (milkshake), after which postprandial levels of DCA and gut hormones (GLP-1 and PYY) were assessed for 8 h. The oLTT challenge was administered at day −1 (as baseline) and at day 15 at the end of the dosing interval (i.e., 8, 12, and 24 h after dosing). The postprandial excursions of biomarkers were evaluated with AUC (0–8 h) during oLTT. Placebos from three dose groups were pooled for the analysis. The percent change from baseline of AUC (0–8 h) for DCA C18:1 during oLTT at day 15 is shown in Figure 7B. There was a significant increase in DCA C18:1 concentration following oLTT meal administered at 8 and 12 h post-BMS-963272 dosing in active treatment regimens while a lesser increase in DCA C18:1 concentration was observed when the oLTT was given 24 h post-dose at the end of Q24H dosing interval. The lower increase in DCA for the Q24H dosing regimen (41%) was consistent with the low C_{trough} of BMS-963272 (6.7 ng/mL). A much higher DCA increase of 177% and 132%, at corresponding C_{trough} values of 39 ng/mL and 91 ng/mL, was observed for the Q12H and Q8H dosing regimens, respectively. These data suggest the need for sufficiently high concentrations of BMS-963272 at trough to ensure complete inhibition of MGAT2 throughout the entire dosing interval to maximize PD response.

Similarly, a significant increase in postprandial PYY during oLTT was observed at 8, 12, and 24 h post-BMS-963272 treatment compared to placebo (Figure 7C). In addition, an increase
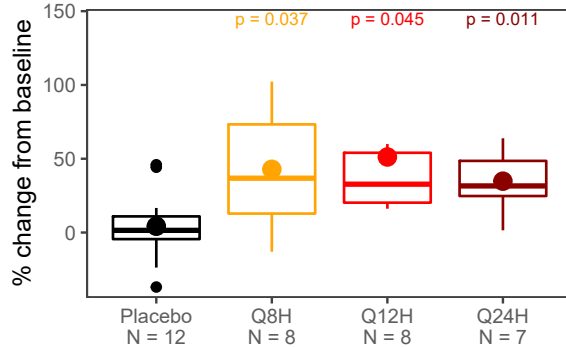
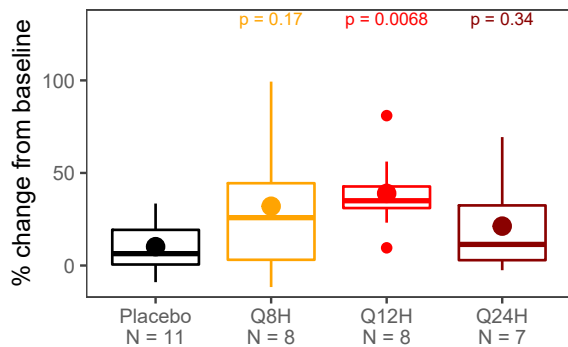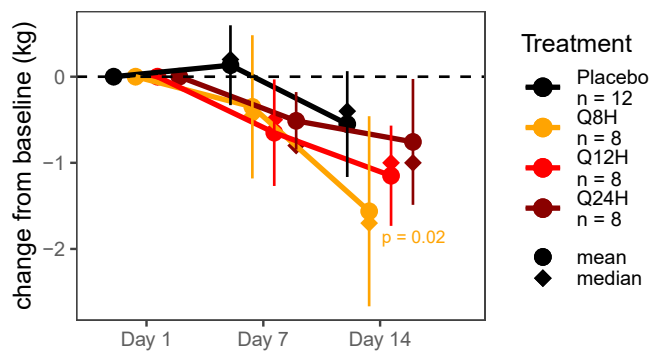**A** Trough concentrations of BMS−963272
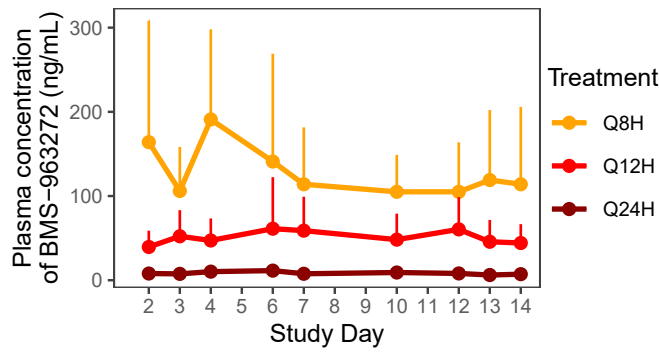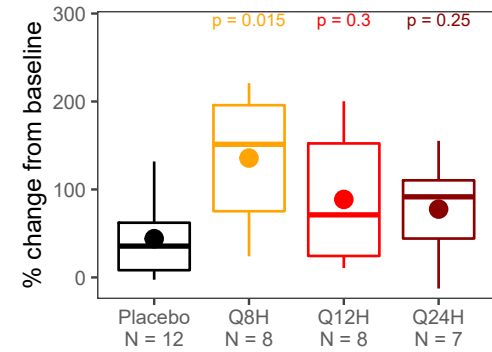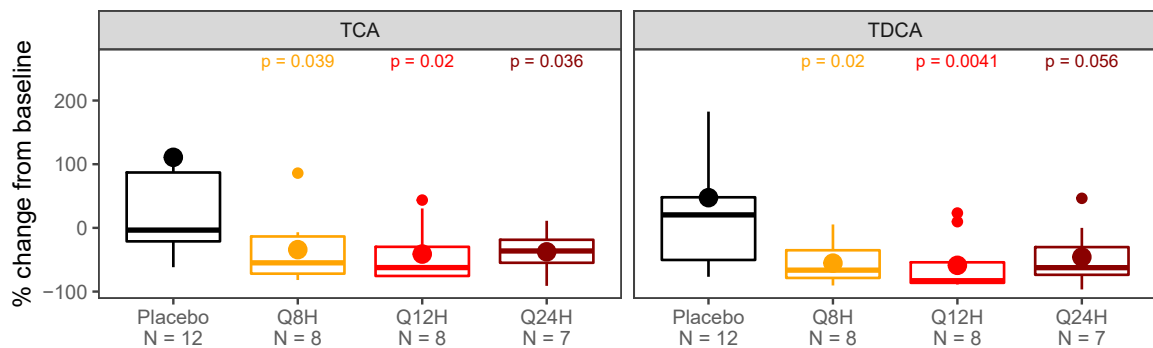
B DCA 18:1
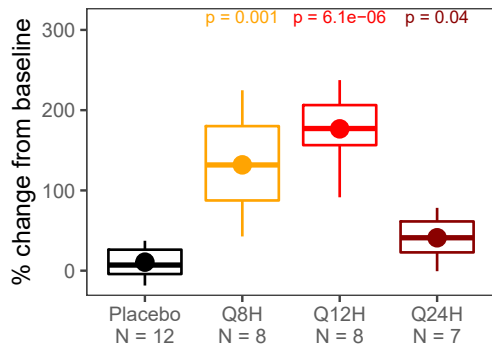
C PYY

D GLP−1

E Weight

F FGF21

G Conjugated bile acids

(legend on next page)

in postprandial GLP-1 was noted in the Q12H treatment group, with a trend toward increase in the Q8H and Q24H treatment groups compared to placebo (Figure 7D). A smaller trend of a decrease in postprandial TG and FFA was observed (data not shown).

BMS-963272 administration in adults with obesity was associated with decreases in body weight and plasma bile acids and an increase in FGF21

A reduction in body weight and BMI was noted from day 7 through day 14 in the Q8H dose group compared with that of pooled placebo, with a smaller trend observed in the Q12H group (Figure 7E). Data for satiety/appetite based on visual analytical scores (VASs) were variable, with a general trend toward increased satiety and decreased appetite in the Q12H and Q8H groups (data not shown).

To explore the potential effects of BMS-963272 on modulating biomarkers involved in NASH pathophysiology, plasma FGF21 and bile acids were evaluated at baseline and day 14 in this study. Analysis of percent change from baseline showed that FGF21 concentrations were increased at day 14 in the Q8H treatment group (median 151%) compared to placebo, with smaller trends toward an increase in the other two treatment groups (Figure 7F). Last, plasma levels of free bile acids (cholic acid, deoxycholic acid, and chenodeoxycholic acid) and conjugated forms of these bile acids (glycocholic acid, taurocholic acid [TCA], glycodeoxycholic acid, taurodeoxycholic acid [TDCA], glycochenodeoxycholic acid, and taurochenodeoxycholic acid) were measured in this study at fasted state at day 1 (baseline) and day 14. While no consistent treatment-related changes were observed for free bile acids, a reduction was observed for conjugated bile acids, including glycocholic acid, TCA, glycodeoxycholic acid, TDCA, and taurochenodeoxycholic acid on day 14 for all 3 active treatment groups compared with placebo. Percent change from baseline for TCA and TDCA is shown in Figure 7G.

DISCUSSION

MGAT2 is an emerging target for the treatment of metabolic disorders such as obesity and NASH. But traditionally MGAT2 has been considered a purely metabolic target due to its function in TG metabolism. Inhibition of MGAT2 is associated with weight loss through the regulation of gut hormones and energy expenditure (Shi and Cheng, 2009; Yen et al., 2009). The potential for MGAT2 inhibition-mediated NASH treatment was postulated to occur through a decrease in steatosis. Indeed, along with weight loss, *Mogat2* knockout (KO) mice showed decreased liver TG to <5% of WT after 8 months of HFD challenge in diet-induced obese (DIO) mice (Yen et al., 2009). Take et al. reported that pharmacological treatment of MGAT2 selective inhibitor compound A significantly decreased liver TG content in an HFD-STZ model (Take et al., 2016). Using an analog of BMS-963272, we also found that treatment with MGAT2 inhibitor in HFD-STZ mice led to a reduction of liver TG content by ~50% that was associated with weight loss (data not shown).

In the current study, we found MGAT2 inhibition goes beyond purely metabolic effects. BMS-963272 decreased inflammation and fibrosis independent of liver TG content in CDAHFD and STAM mice. Of interest, oleamide, an endocannabinoid found to be increased by BMS-963272 in the liver of STAM mice, led to an apoptotic effect on activated HSCs *in vitro*, suggesting its direct role in anti-fibrosis. Second, we found multiple inflammation-resolving HETE molecules were increased in the intestine through the induction of *Cyp2c29* and *Cyp2c65* by BMS-963272. The decrease of inflammation in intestine may contribute to the decrease of inflammation in the NASH models. Third, RNA-seq studies revealed that multiple fibrosis and inflammation pathways were downregulated in the CDAHFD liver and intestine by BMS-963272. Furthermore, in Phase 1 human trials, BMS-963272 was generally safe and well tolerated. In the 14-day Phase 1 study in healthy human adults with obesity, BMS-963272 decreased body weight, which may be partially explained by the elevation of gut hormone PYY and GLP-1 levels. Last, we report that increase of long-chain DCAs, an intermediate product of ω-fatty acid oxidation that are readily detectable in circulation, can serve as a specific translational PD biomarker for MGAT2 inhibitors. Taken together, we suggest that these findings represent a major advance supporting the hypothesis that MGAT2 inhibitors may be promising for the treatment of NAFLD and NASH. Targeting MGAT2 may synergize anti-fibrotic and anti-inflammatory effects with beneficial metabolic effects in the liver. The implications of our data and limitations of current studies are discussed below.

Comparison of MGAT2 with DGAT1 and DGAT2

GI effects, most notably diarrhea, led to the discontinuation of development of several DGAT1 inhibitors (Denison et al., 2014; DeVita and Pinto, 2013). Our results of a Phase 1 clinical study of BMS-963272 indicate that MGAT2 inhibitors may present improved GI tolerability relative to DGAT1 inhibitors. In the 14-day BMS-963272 study in healthy adults with obesity, mild diarrhea was observed in 25% of subjects who received BMS-963272, but it did not lead to treatment discontinuation. Of note, there were no overall changes in the daily number of bowel

---

Figure 7. BMS-963272 PK and PD responses in human adults with obesity after 14-day treatment
(A) Trough concentrations of BMS-963272, mean + SD.
(B–D) DCA 18:1 (B), PYY (C), and GLP-1% change from baseline for AUC (0–8 h) (D). Mean (large dot), median ± interquartile range (IQR) (box), and furthest point ≤ 1.5*IQR (whiskers). p values reflect Welch's two-sample test comparing percent change from baseline for each treated group to pooled placebo.
(E) Weight (kg) change from baseline, mean ± SEM. p values reflect a linear mixed model comparing the change in each treated group to the change in placebo at day 14 relative to baseline (STAR Methods).
(F) FGF21 percent change from baseline. Mean (large dot), median ± IQR (box), and furthest point ≤ 1.5*IQR (whiskers). p values reflect pairwise Mann-Whitney U tests comparing percent change from baseline for each treated group to pooled placebo.
(G) Conjugated bile acid percent change from baseline. Mean (large dot), median ± IQR (box), and furthest point ≤ 1.5*IQR (whiskers). 1–2 outliers in placebo groups >2 SD above the mean not shown (summary statistics reflect the totality of the data). p values reflect pairwise Mann-Whitney U tests comparing percent change from baseline for each treated group to pooled placebo.

movements. This is in distinct contrast to the report by Denison et al. that 11/18 subjects treated with DGAT1 inhibitor AZD7687 withdrew from the shorter (1 week) study due to GI intolerance (Denison et al., 2014).

We hypothesize that the difference in the GI tolerability is attributed to the differences in substrate recognition between MGAT2 and DGAT1. Despite its nomenclature, DGAT1 also recognizes MG substrates (Cheng et al., 2008; Yen et al., 2005). In addition, in higher species such as humans, monkeys, and dogs, MGAT3 is highly expressed in the intestine and catalyzes the MGAT reaction (Cheng et al., 2003). Thus, in the enterocyte of the small intestine, MGAT2 is not the exclusive enzyme for catalyzing the MGAT reaction. MGAT2 inhibition may only cause a partial reduction or delay, rather than a blockade, of TG absorption.

In HFD-fed cynomolgus monkeys, we tested the GI effects of DGAT1 inhibitor PF-04620110, which was previously studied in human subjects (Maciejewski et al., 2013). Within 4 days, at 0.3 and 1 mg/kg/day doses, at plasma concentrations comparable to those that caused diarrhea in clinical trials (Maciejewski et al., 2013), PF-04620110 also caused diarrhea in the cynomolgus monkeys. In contrast, in the same model, doses of 1 and 10 mg/kg/day BMS-963272 (with 2.8- to 3.9-fold efficacious AUC of 0.3 mg/kg in C57Bl/6 mouse models) did not cause diarrhea/unformed feces within 4 days. These results are consistent with the clinical observations that MGAT2 inhibitor BMS-963272 has improved GI tolerability relative to DGAT1 inhibitors. Consistent with the lack of diarrhea in cynomolgus monkeys, quantitative fecal analysis of mice treated with BMS-963272 under the challenge of HFD did not reveal fat malabsorption and increase of stool TG (data not shown).

The pharmacological effect of DGAT2 inhibition was also tested in the methionine- and choline-deficient diet (MCD)-fed db/db mice, a murine NASH model with β cell failure. In contrast to our findings with the MGAT2 inhibitor in the CDAHFD model (which is also methionine and choline deficient), DGAT2 ASO dramatically decreased steatosis but increased necroinflammation and fibrosis, potentially due to increased hepatic FFAs and lipid peroxidation and oxidant stress (Yamaguchi et al., 2007).

In both CDAHFD and STAM mice, BMS-963272 reduced inflammation and fibrosis without changes in liver TG. CDAHFD and STAM mice bear significant differences from HFD-induced DIO and HFD-STZ models. CDAHFD mice are fed a diet deficient in both methionine and choline and hence are significantly underweight (Matsumoto et al., 2013). STAM mice are also underweight as they resemble the human type 1 diabetic condition whereby pancreatic insulin production is diminished 2 days after birth by the injection of STZ (Fujii et al., 2013). Consequently, BMS-963272 failed to reduce the body weight further in both models. We hypothesize that the lack of body weight reduction (which would reduce the adiposity and thereby reduce the FFA flux to the liver TG) may be the key reason why there is no reduction in liver TG by BMS-963272 in these two murine NASH models.

Long-chain fatty acid DCAs as a biomarker for MGAT2 inhibitors

The discovery of long-chain DCAs as a biomarker for MGAT2 inhibition stemmed from multiple whole-genome RNA expression profiling efforts where we found *cyp4a* genes were upregulated in the small intestine and liver. The Cyp4A enzymes catalyze ω-fatty acid oxidation to produce DCAs that are secreted in the circulation. Detecting long-chain DCAs in plasma and liver tissue provides evidence of target engagement of inhibition of MGAT2 in STAM mice (Figure 5). Similar results were also obtained in the CDAHFD model (data not shown). Importantly, in a thioacetamide (TAA)-induced rat liver fibrosis model (a liver toxin-based rather than high-fat-driven model), BMS-963272 failed to increase DCAs and did not decrease fibrosis (data not shown), indicating that target engagement in the liver is important for the anti-fibrotic effect. The most notable difference between plasma and liver was observed with C20:4 and C18:2 DCAs. In the plasma, both C20:4 and C18:2 DCAs were significantly elevated (Figure 5D). In contrast, in the liver tissue, C20:4 DCA was not detectable and C18:2 was decreased by BMS-963272 (Figure 5E). We hypothesize that the elevation of C20:4 and C18:2 DCAs in plasma might reflect inhibition of intestinal MGAT2 where fatty acid species are more reflective of diet, unlike liver.

Three lines of evidence indicate that long-chain DCA elevation in response to BMS-963272 treatment is through MGAT2 inhibition. First, only long-chain fatty acids (chain length > 16 carbons) were found to be elevated (Figures 1 and 5), which is consistent with the enzymatic feature of MGAT2 favoring long fatty-acyl Co-As as substrates (data not shown). Second, *Mogat2*$^{-/-}$ mice (a genetic depletion of MGAT2 enzyme) also exhibited increased long DCAs. Third, treatment of *Mogat2*$^{-/-}$ mice with BMS-963272 did not further increase DCA levels, indicating that BMS-963272-mediated DCA increases are through the MGAT2-inhibitory mechanism (Figure 1G).

Apoptotic effect of oleamide on activated HSCs

Another class of fatty acid-derived metabolite detected in the STAM mice upon the treatment of BMS-963272 is fatty acid amides (Figure 5F). Among them, the most abundant species appears to be oleamide. Consistent with its reported endocannabinoid activity (De Petrocellis et al., 2000), oleamide also caused an apoptotic effect on activated HSCs *in vitro*, similar to the anti-fibrotic endocannabinoid 2-AG and methanandamide, a stable analog of endocannabinoid anandamide (Julien et al., 2005). An RT-PCR experiment revealed that *MOGAT2* is specifically expressed in hepatocytes, but not in HSCs, endothelial cells, or Kupffer cells (data not shown), suggesting that the most likely candidate cell type that generates oleamides in the liver is hepatocytes. Driscoll et al. reported that purified cytochrome *c* directly catalyzes the synthesis of oleamide *in vitro* (Driscoll et al., 2007). Inasmuch as cytochrome *c* released from mitochondria initiates the caspase activation pathway that results in apoptosis (Jiang and Wang, 2004; Liu et al., 1996), it is possible that in NASH, the injured hepatocytes have increased cytosolic cytochrome *c* released from mitochondria that catalyzes the formation of oleamide, which might be readily accessible to the neighboring HSCs. Consistent with this hypothesis, recently Li et al. reported that oleamide might be a serum biomarker for liver injury due to chronic hepatitis B virus infection (Li et al., 2021).

Due to the limitation of metabolomic technology, our current finding of oleamide elevation in the STAM mouse liver does not

provide its quantitative measurement of tissue concentration. Therefore, the direct connection of *in vivo* oleamide concentration with *in vitro* apoptotic effect on HSCs remains to be established. However, Li et al. reported that the optimal cut-off value of oleamide serum concentration in patients with liver cirrhosis and HCC is 23.6 mg/L (equivalent to 80 μM) (Li et al., 2021), a concentration within the range of effective HSC apoptotic concentration of oleamide *in vitro* (Figure 5G).

Regulation of liver and intestinal gene expression by MGAT2 inhibition

RNA-seq profiling in the CDAHFD liver identified a number of genes involved in the fibrosis and inflammatory pathways that were downregulated by BMS-963272. These elucidate several mechanisms behind the mouse phenotypes observed: (1) downregulation of THBS1-mediated/TGF-β-induced liver injury, inflammation, and fibrosis; (2) downregulation of PTGS2-mediated inflammation in the liver; (3) upregulation of fatty acid oxidation in the intestine; (4) downregulation of Th17 chemokines and matrix metalloproteinases induced by epithelial injury in the intestine; and (5) upregulation of Cyp2C to activate xenobiotic and HETE/EET inflammation-resolving pathway in the intestine. The most highly downregulated fibrosis gene in the liver was THBS1 (−2-fold, p = 0.0018) (Table S2). THBS1 (encoding thrombospondin 1) activates latent TGF-β (Murphy-Ullrich and Suto, 2018), the master cytokine that plays profound roles in all stages of liver disease progression, beginning with the initial liver injury that leads to the development of inflammation and fibrosis (Fabregat et al., 2016). Another highly downregulated gene in the liver is PTGS2, also known as COX2 (−1.8-fold, p = 0.0099) (Table S2). Unlike COX1, PTGS2 is not expressed under normal physiological conditions but is elevated during inflammation. PTGS2 encodes the prostaglandin-endoperoxide synthase 2 enzyme that converts arachidonic acid into prostaglandin endoperoxide H2, thus mediating the inflammatory responses (Williams et al., 1999). The significance of PTGS2 involvement in the inflammatory process is highlighted by the fact that multiple PTGS2 inhibitors are effective for the treatment of a variety of inflammatory indications (Hochberg, 2005). Direct involvement of PTGS2 in liver inflammation and carcinogenesis was also suggested recently (Martin-Sanz et al., 2017).

In the jejunum, pleiotropic mechanisms seem to have been activated by MGAT2 inhibition. First, fatty acid oxidation genes exhibited striking upregulation. Our results are consistent with the results by Take et al. where they discovered MGAT2 inhibition increased the level of acyl-carnitine with shorter acyl chains, the intermediate products of fatty acid oxidation (Take et al., 2016). In addition, several inflammatory pathways and genes were also found be downregulated by BMS-963272. The most highly downregulated inflammatory genes by BMS-963272 were Ccl8 (−2-fold, p = 0.064) and Cxcl10 (−1.8-fold, p = 0.074) (Table S3). Interestingly, both Ccl8 and Cxcl10 are chemokines induced under inflammatory intestinal conditions where the epithelial mucosal barrier is compromised (Zimmerman et al., 2008).

Implications of BMS-963272 for the treatment of NASH

The biomarker data from the 14-day Phase I trial suggest potential beneficial effects of MGAT2 inhibition in patients with NASH.

Elevation of postprandial PYY and GLP-1 may have contributed to the reduction in body weight observed in humans following the administration of BMS-963272. It has previously been reported that weight loss of >10% over 52 weeks was associated with NASH resolution and fibrosis regression (Vilar-Gomez et al., 2015) and weight loss of >5% over 24 weeks was associated with 15%–19% relative reduction in liver stiffness measured by magnetic resonance elastography (Patel et al., 2017). The extent of weight loss observed following 14 days of administration of BMS-963272 at 300 mg Q12H (−1.0 kg) and 300 mg Q8H (−1.7 kg) was similar to that reported for Exenatide after 2-week treatment (−0.8 kg) (Dushay et al., 2012). This suggests that inhibition of MGAT2 by BMS-963272 may reduce body weight and improve metabolic functions. Notably, body weight tended to decrease in Q24H and Q12H groups; a significant decrease was only observed for the Q8H group (p = 0.02) (Figure 7E). The magnitude and durability of body weight reductions in patients remain to be investigated in longer-duration studies with larger sample sizes.

In addition, an increase in plasma FGF21 was observed after administration of BMS-963272 for 2 weeks. FGF21 elevation associated with BMS-963272 administration may be beneficial for NASH patients. FGF21 mimetics have demonstrated NASH resolution, fibrosis regression, and robust reduction in fatty liver and fibrogenic biomarkers (Harrison et al., 2021; Sanyal et al., 2019). The elevation of FGF21 in humans was consistent with the observed elevation of liver *Fgf21* gene expression in CDAHFD mice (Table S2).

Limitations of study

There are several important limitations to our current study. First, the limitations of the Phase 1 study in healthy human adults with obesity include the brevity of study duration and the small sample size. Further investigations of BMS-963272 in patients with NASH are thus warranted. Second, BMS-963272 has a short half-life in humans and twice- or thrice-daily dose regimens may be needed to achieve desired effects. MGAT2 inhibitors with an improved PK profile could offer potential for a once-daily regimen that is sufficient to provide MGAT2 target coverage over a 24 h duration. Third, mechanistic understandings of how MGAT2 inhibition mediates anti-inflammatory and anti-fibrotic liver effects deserve further exploration. One of the limitations of our metabolomic technology is that it only reflects changes of relative, not absolute, levels of oleamide in liver tissues. Furthermore, there is no precedent literature report of methods for the quantitative measurement of oleamide in tissue. Thus, the correlation of *in vivo* tissue level of oleamide with its *in vitro* apoptotic effects on the activated HSCs remain to be established. Last, the low DCA PK exposure precludes us from directly testing the hypothesis that DCA may causally mediate anti-inflammation and anti-fibrosis in mouse NASH models. Further understanding of all these mechanisms could uncover additional synergistic molecular targets for the treatment of NASH.

STAR★METHODS

Detailed methods are provided in the online version of this paper and include the following:

- **RESOURCE AVAILABILITY**
  - Lead contact
  - Materials availability
  - Data and code availability
- **EXPERIMENTAL MODEL AND SUBJECT DETAILS**
  - Ethical statements
  - Preclinical models
  - Human studies
  - Evaluation of PK parameters
  - Evaluation of biomarkers in phase 1 study
  - Safety assessments
  - Statistical methods
- **METHOD DETAILS**
  - Mouse plasma TNFα measurement
  - RNA-seq study
  - Apoptotic effect of oleamide on human HSC
  - Metabolomic evaluation of plasma and liver samples from BMS-963272 treated STAM mice
  - Measurement of small intestinal HETE and EET

REFERENCES

Adam, R., Karam, V., Cailliez, V., O Grady, J.G., Mirza, D., Cherqui, D., Klempnauer, J., Salizzoni, M., Pratschke, J., Jamieson, N., et al. (2018). 2018 Annual Report of the European Liver Transplant Registry (ELTR) - 50-year evolution of liver transplantation. Transpl. Int. *31*, 1293–1317. https://doi.org/10.1111/tri.13358.

Angulo, P., Kleiner, D.E., Dam-Larsen, S., Adams, L.A., Bjornsson, E.S., Charatcharoenwitthaya, P., Mills, P.R., Keach, J.C., Lafferty, H.D., Stahler, A., et al. (2015). Liver fibrosis, but no other histologic features, is associated with long-term outcomes of patients with nonalcoholic fatty liver disease. Gastroenterology *149*, 389–397.e10. https://doi.org/10.1053/j.gastro.2015.04.043.

Burra, P., Becchetti, C., and Germani, G. (2020). NAFLD and liver transplantation: disease burden, current management and future challenges. JHEP Rep. *2*, 100192. https://doi.org/10.1016/j.jhepr.2020.100192.

Cao, J., Lockwood, J., Burn, P., and Shi, Y. (2003). Cloning and functional characterization of a mouse intestinal acyl-CoA:monoacylglycerol acyltransferase, MGAT2. J. Biol. Chem. *278*, 13860–13866. https://doi.org/10.1074/jbc.m300139200.

Cheng, D., Nelson, T.C., Chen, J., Walker, S.G., Wardwell-Swanson, J., Meegalla, R., Taub, R., Billheimer, J.T., Ramaker, M., and Feder, J.N. (2003). Identification of acyl coenzyme A:monoacylglycerol acyltransferase 3, an intestinal specific enzyme implicated in dietary fat absorption. J. Biol. Chem. *278*, 13611–13614. https://doi.org/10.1074/jbc.c300042200.

Cheng, D., Iqbal, J., Devenny, J., Chu, C.H., Chen, L., Dong, J., Seethala, R., Keim, W.J., Azzara, A.V., Lawrence, R.M., et al. (2008). Acylation of acylglycerols by acyl coenzyme A:diacylglycerol acyltransferase 1 (DGAT1). J. Biol. Chem. *283*, 29802–29811. https://doi.org/10.1074/jbc.m800494200.

Cohen, J.C., Horton, J.D., and Hobbs, H.H. (2011). Human fatty liver disease: old questions and new insights. Science *332*, 1519–1523. https://doi.org/10.1126/science.1204265.

Cotter, T.G., and Charlton, M. (2020). Nonalcoholic steatohepatitis after liver transplantation. Liver Transpl. *26*, 141–159. https://doi.org/10.1002/lt.25657.

De Petrocellis, L., Melck, D., Bisogno, T., and Di Marzo, V. (2000). Endocannabinoids and fatty acid amides in cancer, inflammation and related disorders. Chem. Phys. Lipids *108*, 191–209. https://doi.org/10.1016/s0009-3084(00)00196-1.

Denison, H., Nilsson, C., Lofgren, L., Himmelmann, A., Martensson, G., Knutsson, M., Al-Shurbaji, A., Tornqvist, H., and Eriksson, J.W. (2014). Diacylglycerol acyltransferase 1 inhibition with AZD7687 alters lipid handling and hormone secretion in the gut with intolerable side effects: a randomized clinical trial. Diabetes Obes. Metab. *16*, 334–343. https://doi.org/10.1111/dom.12221.

DeVita, R.J., and Pinto, S. (2013). Current status of the research and development of diacylglycerol O-acyltransferase 1 (DGAT1) inhibitors. J. Med. Chem. *56*, 9820–9825. https://doi.org/10.1021/jm4007033.

Donnelly, K.L., Smith, C.I., Schwarzenberg, S.J., Jessurun, J., Boldt, M.D., and Parks, E.J. (2005). Sources of fatty acids stored in liver and secreted via lipoproteins in patients with nonalcoholic fatty liver disease. J. Clin. Invest. *115*, 1343–1351. https://doi.org/10.1172/jci23621.

Dow, R.L., Li, J.C., Pence, M.P., Gibbs, E.M., LaPerle, J.L., Litchfield, J., Piotrowski, D.W., Munchhof, M.J., Manion, T.B., Zavadoski, W.J., et al. (2011). Discovery of PF-04620110, a potent, selective, and orally bioavailable inhibitor of DGAT-1. ACS Med. Chem. Lett. *2*, 407–412. https://doi.org/10.1021/ml200051p.

Driscoll, W.J., Chaturvedi, S., and Mueller, G.P. (2007). Oleamide synthesizing activity from rat kidney: identification as cytochrome c. J. Biol. Chem. *282*, 22353–22363. https://doi.org/10.1074/jbc.m610070200.

Dushay, J., Gao, C., Gopalakrishnan, G.S., Crawley, M., Mitten, E.K., Wilker, E., Mullington, J., and Maratos-Flier, E. (2012). Short-term exenatide treatment leads to significant weight loss in a subset of obese women without diabetes. Diabetes Care *35*, 4–11. https://doi.org/10.2337/dc11-0931.

Esler, W.P., and Bence, K.K. (2019). Metabolic targets in nonalcoholic fatty liver disease. Cell Mol. Gastroenterol. Hepatol. *8*, 247–267. https://doi.org/10.1016/j.jcmgh.2019.04.007.

Estes, C., Razavi, H., Loomba, R., Younossi, Z., and Sanyal, A.J. (2018). Modeling the epidemic of nonalcoholic fatty liver disease demonstrates an

exponential increase in burden of disease. Hepatology *67*, 123–133. https://doi.org/10.1002/hep.29466.

Fabregat, I., Moreno-Caceres, J., Sanchez, A., Dooley, S., Dewidar, B., Giannelli, G., Ten Dijke, P., and IT-LIVER Consortium. (2016). TGF-beta signalling and liver disease. FEBS J. *283*, 2219–2232. https://doi.org/10.1111/febs.13665.

Fujii, M., Shibazaki, Y., Wakamatsu, K., Honda, Y., Kawauchi, Y., Suzuki, K., Arumugam, S., Watanabe, K., Ichida, T., Asakura, H., and Yoneyama, H. (2013). A murine model for non-alcoholic steatohepatitis showing evidence of association between diabetes and hepatocellular carcinoma. Med. Mol. Morphol. *46*, 141–152. https://doi.org/10.1007/s00795-013-0016-1.

Hall, A.M., Kou, K., Chen, Z., Pietka, T.A., Kumar, M., Korenblat, K.M., Lee, K., Ahn, K., Fabbrini, E., Klein, S., et al. (2012). Evidence for regulated monoacylglycerol acyltransferase expression and activity in human liver. J. Lipid Res. *53*, 990–999. https://doi.org/10.1194/jlr.p025536.

Hardwick, J.P. (2008). Cytochrome P450 omega hydroxylase (CYP4) function in fatty acid metabolism and metabolic diseases. Biochem. Pharmacol. *75*, 2263–2275. https://doi.org/10.1016/j.bcp.2008.03.004.

Harrison, S.A., Ruane, P.J., Freilich, B.L., Neff, G., Patil, R., Behling, C.A., Hu, C., Fong, E., de Temple, B., Tillman, E.J., et al. (2021). Efruxifermin in non-alcoholic steatohepatitis: a randomized, double-blind, placebo-controlled, phase 2a trial. Nat. Med. *27*, 1262–1271. https://doi.org/10.1038/s41591-021-01425-3.

Hirasawa, A., Tsumaya, K., Awaji, T., Katsuma, S., Adachi, T., Yamada, M., Sugimoto, Y., Miyazaki, S., and Tsujimoto, G. (2005). Free fatty acids regulate gut incretin glucagon-like peptide-1 secretion through GPR120. Nat. Med. *11*, 90–94. https://doi.org/10.1038/nm1168.

Hochberg, M. (2005). COX-2 selective inhibitors in the treatment of arthritis: a rheumatologist perspective. Curr. Top. Med. Chem. *5*, 443–448. https://doi.org/10.2174/1568026054201695.

Jiang, X., and Wang, X. (2004). Cytochrome *c*-mediated apoptosis. Annu. Rev. Biochem. *73*, 87–106. https://doi.org/10.1146/annurev.biochem.73.011303.073706.

Julien, B., Grenard, P., Teixeira-Clerc, F., Van Nhieu, J.T., Li, L., Karsak, M., Zimmer, A., Mallat, A., and Lotersztajn, S. (2005). Antifibrogenic role of the cannabinoid receptor CB2 in the liver. Gastroenterology *128*, 742–755. https://doi.org/10.1053/j.gastro.2004.12.050.

Kleiner, D.E., Brunt, E.M., Van Natta, M., Behling, C., Contos, M.J., Cummings, O.W., Ferrell, L.D., Liu, Y.C., Torbenson, M.S., Unalp-Arida, A., et al. (2005). Design and validation of a histological scoring system for nonalcoholic fatty liver disease. Hepatology *41*, 1313–1321. https://doi.org/10.1002/hep.20701.

Konerman, M.A., Jones, J.C., and Harrison, S.A. (2018). Pharmacotherapy for NASH: Current and emerging. J. Hepatol. *68*, 362–375. https://doi.org/10.1016/j.jhep.2017.10.015.

Lassailly, G., Caiazzo, R., Buob, D., Pigeyre, M., Verkindt, H., Labreuche, J., Raverdy, V., Leteurtre, E., Dharancy, S., Louvet, A., et al. (2015). Bariatric surgery reduces features of nonalcoholic steatohepatitis in morbidly obese patients. Gastroenterology *149*, 379–388. https://doi.org/10.1053/j.gastro.2015.04.014.

Li, H., Wang, Y., Ma, S., Zhang, C., Liu, H., and Sun, D. (2021). Clinical significance of small molecule metabolites in the blood of patients with different types of liver injury. Sci. Rep. *11*, 11642. https://doi.org/10.1038/s41598-021-91164-9.

Little, T.J., Russo, A., Meyer, J.H., Horowitz, M., Smyth, D.R., Bellon, M., Wishart, J.M., Jones, K.L., and Feinle-Bisset, C. (2007). Free fatty acids have more potent effects on gastric emptying, gut hormones, and appetite than triacylglycerides. Gastroenterology *133*, 1124–1131. https://doi.org/10.1053/j.gastro.2007.06.060.

Liu, X., Kim, C.N., Yang, J., Jemmerson, R., and Wang, X. (1996). Induction of apoptotic program in cell-free extracts: requirement for dATP and cytochrome c. Cell *86*, 147–157. https://doi.org/10.1016/s0092-8674(00)80085-9.

Luo, G., Zeldin, D.C., Blaisdell, J.A., Hodgson, E., and Goldstein, J.A. (1998). Cloning and expression of murine CYP2Cs and their ability to metabolize

arachidonic acid. Arch. Biochem. Biophys. *357*, 45–57. https://doi.org/10.1006/abbi.1998.0806.

Maciejewski, B.S., LaPerle, J.L., Chen, D., Ghosh, A., Zavadoski, W.J., McDonald, T.S., Manion, T.B., Mather, D., Patterson, T.A., Hanna, M., et al. (2013). Pharmacological inhibition to examine the role of DGAT1 in dietary lipid absorption in rodents and humans. Am. J. Physiol. Gastrointest. Liver Physiol. *304*, G958–G969. https://doi.org/10.1152/ajpgi.00384.2012.

Martin-Sanz, P., Casado, M., and Bosca, L. (2017). Cyclooxygenase 2 in liver dysfunction and carcinogenesis: facts and perspectives. World J. Gastroenterol. *23*, 3572. https://doi.org/10.3748/wjg.v23.i20.3572.

Matsumoto, M., Hada, N., Sakamaki, Y., Uno, A., Shiga, T., Tanaka, C., Ito, T., Katsume, A., and Sudoh, M. (2013). An improved mouse model that rapidly develops fibrosis in non-alcoholic steatohepatitis. Int. J. Exp. Pathol. *94*, 93–103. https://doi.org/10.1111/iep.12008.

Mosteller, R.D. (1987). Simplified calculation of body-surface area. N. Engl. J. Med. *317*, 1098. https://doi.org/10.1056/NEJM198710223171717.

Murphy-Ullrich, J.E., and Suto, M.J. (2018). Thrombospondin-1 regulation of latent TGF-beta activation: a therapeutic target for fibrotic disease. Matrix Biol. *68–69*, 28–43. https://doi.org/10.1016/j.matbio.2017.12.009.

Patel, N.S., Hooker, J., Gonzalez, M., Bhatt, A., Nguyen, P., Ramirez, K., Richards, L., Rizo, E., Hernandez, C., Kisseleva, T., et al. (2017). Weight loss decreases magnetic resonance elastography estimated liver stiffness in nonalcoholic fatty liver disease. Clin. Gastroenterol. Hepatol. *15*, 463–464. https://doi.org/10.1016/j.cgh.2016.09.150.

Promrat, K., Kleiner, D.E., Niemeier, H.M., Jackvony, E., Kearns, M., Wands, J.R., Fava, J.L., and Wing, R.R. (2010). Randomized controlled trial testing the effects of weight loss on nonalcoholic steatohepatitis. Hepatology *51*, 121–129. https://doi.org/10.1002/hep.23276.

Sanyal, A.J., Friedman, S.L., McCullough, A.J., Dimick-Santos, L., American Association for the Study of Liver Diseases, and United States Food and Drug Administration. (2015). Challenges and opportunities in drug and biomarker development for nonalcoholic steatohepatitis: findings and recommendations from an American Association for the Study of Liver Diseases-U.S. Food and Drug Administration Joint Workshop. Hepatology *61*, 1392–1405. https://doi.org/10.1002/hep.27678.

Sanyal, A., Charles, E.D., Neuschwander-Tetri, B.A., Loomba, R., Harrison, S.A., Abdelmalek, M.F., Lawitz, E.J., Halegoua-DeMarzio, D., Kundu, S., Noviello, S., et al. (2018). Pegbelfermin (BMS-986036), a PEGylated fibroblast growth factor 21 analogue, in patients with non-alcoholic steatohepatitis: a randomised, double-blind, placebo-controlled, phase 2a trial. Lancet *392*, 2705–2717. https://doi.org/10.1016/s0140-6736(18)31785-9.

Serhan, C.N., Chiang, N., and Van Dyke, T.E. (2008). Resolving inflammation: dual anti-inflammatory and pro-resolution lipid mediators. Nat. Rev. Immunol. *8*, 349–361. https://doi.org/10.1038/nri2294.

Shi, Y., and Cheng, D. (2009). Beyond triglyceride synthesis: the dynamic functional roles of MGAT and DGAT enzymes in energy metabolism. Am. J. Physiol. Endocrinol. Metab. *297*, E10–E18. https://doi.org/10.1152/ajpendo.90949.2008.

Slee, E.A., Harte, M.T., Kluck, R.M., Wolf, B.B., Casiano, C.A., Newmeyer, D.D., Wang, H.G., Reed, J.C., Nicholson, D.W., Alnemri, E.S., et al. (1999). Ordering the cytochrome c-initiated caspase cascade: hierarchical activation of caspases-2, -3, -6, -7, -8, and -10 in a caspase-9-dependent manner. J. Cell Biol. *144*, 281–292. https://doi.org/10.1083/jcb.144.2.281.

Suga, T., Yamaguchi, H., Ogura, J., Shoji, S., Maekawa, M., and Mano, N. (2019). Altered bile acid composition and disposition in a mouse model of non-alcoholic steatohepatitis. Toxicol. Appl. Pharmacol. *379*, 114664. https://doi.org/10.1016/j.taap.2019.114664.

Take, K., Mochida, T., Maki, T., Satomi, Y., Hirayama, M., Nakakariya, M., Amano, N., Adachi, R., Sato, K., Kitazaki, T., and Takekawa, S. (2016). Pharmacological inhibition of monoacylglycerol O-acyltransferase 2 improves hyperlipidemia, obesity, and diabetes by change in intestinal fat utilization. PLoS One *11*, e0150976. https://doi.org/10.1371/journal.pone.0150976.

Thornberry, N.A., Rano, T.A., Peterson, E.P., Rasper, D.M., Timkey, T., Garcia-Calvo, M., Houtzager, V.M., Nordstrom, P.A., Roy, S., Vaillancourt, J.P., et al. (1997). A combinatorial approach defines specificities of members of the caspase family and granzyme B. J. Biol. Chem. *272*, 17907–17911. https://doi.org/10.1074/jbc.272.29.17907.

Tsuchida, T., and Friedman, S.L. (2017). Mechanisms of hepatic stellate cell activation. Nat. Rev. Gastroenterol. Hepatol. *14*, 397–411. https://doi.org/10.1038/nrgastro.2017.38.

Turdi, H., Chao, H., Hangeland, J.J., Ahmad, S., Meng, W., Brigance, R., Zhao, G., Wang, W., Moore, F., Ye, X.Y., et al. (2021). Screening hit to clinical candidate: discovery of BMS-963272, a potent, selective MGAT2 inhibitor for the treatment of metabolic disorders. J. Med. Chem. *64*, 14773–14792. https://doi.org/10.1021/acs.jmedchem.1c01356.

Vernon, G., Baranova, A., and Younossi, Z.M. (2011). Systematic review: the epidemiology and natural history of non-alcoholic fatty liver disease and non-alcoholic steatohepatitis in adults. Aliment. Pharmacol. Ther. *34*, 274–285. https://doi.org/10.1111/j.1365-2036.2011.04724.x.

Vilar-Gomez, E., Martinez-Perez, Y., Calzadilla-Bertot, L., Torres-Gonzalez, A., Gra-Oramas, B., Gonzalez-Fabian, L., Friedman, S.L., Diago, M., and Romero-Gomez, M. (2015). Weight loss through lifestyle modification significantly reduces features of nonalcoholic steatohepatitis. Gastroenterology *149*, 367–378.e5. https://doi.org/10.1053/j.gastro.2015.04.005.

Williams, C.S., Mann, M., and DuBois, R.N. (1999). The role of cyclooxygenases in inflammation, cancer, and development. Oncogene *18*, 7908–7916. https://doi.org/10.1038/sj.onc.1203286.

Yamaguchi, K., Yang, L., McCall, S., Huang, J., Yu, X.X., Pandey, S.K., Bhanot, S., Monia, B.P., Li, Y.X., and Diehl, A.M. (2007). Inhibiting triglyceride synthesis improves hepatic steatosis but exacerbates liver damage and fibrosis in obese mice with nonalcoholic steatohepatitis. Hepatology *45*, 1366–1374. https://doi.org/10.1002/hep.21655.

Yang, M., and Nickels, J. (2015). MOGAT2: a new therapeutic target for metabolic syndrome. Diseases *3*, 176–192. https://doi.org/10.3390/diseases3030176.

Yen, C.L.E., and Farese, R.V., Jr. (2003). MGAT2, a monoacylglycerol acyltransferase expressed in the small intestine. J. Biol. Chem. *278*, 18532–18537. https://doi.org/10.1074/jbc.m301633200.

Yen, C.L.E., Monetti, M., Burri, B.J., and Farese, R.V., Jr. (2005). The triacylglycerol synthesis enzyme DGAT1 also catalyzes the synthesis of diacylglycerols, waxes, and retinyl esters. J. Lipid Res. *46*, 1502–1511. https://doi.org/10.1194/jlr.m500036-jlr200.

Yen, C.L.E., Cheong, M.L., Grueter, C., Zhou, P., Moriwaki, J., Wong, J.S., Hubbard, B., Marmor, S., and Farese, R.V., Jr. (2009). Deficiency of the intestinal enzyme acyl CoA:monoacylglycerol acyltransferase-2 protects mice from metabolic disorders induced by high-fat feeding. Nat. Med. *15*, 442–446. https://doi.org/10.1038/nm.1937.

Younossi, Z., Stepanova, M., Ong, J.P., Jacobson, I.M., Bugianesi, E., Duseja, A., Eguchi, Y., Wong, V.W., Negro, F., Yilmaz, Y., et al. (2019). Nonalcoholic steatohepatitis is the fastest growing cause of hepatocellular carcinoma in liver transplant candidates. Clin. Gastroenterol. Hepatol. *17*, 748–755.e3. https://doi.org/10.1016/j.cgh.2018.05.057.

Zimmerman, N.P., Vongsa, R.A., Wendt, M.K., and Dwinell, M.B. (2008). Chemokines and chemokine receptors in mucosal homeostasis at the intestinal epithelial barrier in inflammatory bowel disease. Inflamm. Bowel Dis. *14*, 1000–1011. https://doi.org/10.1002/ibd.20480.

STAR★METHODS

RESOURCE AVAILABILITY

Lead contact
Further information and requests for resources and reagents should be directed to Lead Contact, Dong Cheng (e-mail: dong.cheng@bms.com).

Materials availability
This study did not generate new unique reagents.

Data and code availability
- The RNA-seq datasets have been deposited at EGA. The access numbers for RNA-seq of liver harvested from CDAHFD mice treated for 8 weeks with either the MGAT2 inhibitor BMS-963272 or vehicle are Study ID:EGAS00001006583, Dataset ID:EGAD00001009389 and for RNA-seq of jejunum harvested from CDAHFD mice treated for 8 weeks with either the MGAT2 inhibitor BMS-963272 or vehicle are StudyID:EGAS00001006584, Dataset ID: EGAD00001009390. Original data for creating the graphs in the paper are provided in Data S1.
- This study did not generate any code.
- Any additional information required to reanalyze the data reported in this paper is available from the lead contact upon reasonable request.

EXPERIMENTAL MODEL AND SUBJECT DETAILS

Ethical statements
The clinical studies were conducted in accordance with Good Clinical Practice, as defined by the International Council for Harmonisation and with the ethical principles that have their origin in the Declaration of Helsinki. The protocol, amendments, and participant informed consent were approved by the Institutional Review Board/Independent Ethics Committee prior to the initiation of the study at each site. All participants gave written informed consent prior to study participation.

The animal studies were conducted in accordance with the Japanese Pharmacological Society Guidance for Animal Use (for STAM model) or with Animal Care and Use Committee (ACUC) approved Animal Test Method (ATM) procedures at BMS, Hopewell, NJ (all other animal studies).

Preclinical models
Study of BMS-963272 in CDAHFD model of NASH
C57BL/6J mice, 6 weeks of age, were purchased from Jackson Laboratories (Bar Harbor, ME) and acclimated to the Hopewell BMS animal facility for 1 week on standard rodent chow (Teklad 2018, Madison, WI). At 7 weeks of age mice were placed on either a normal chow diet (Research Diets A13012807, New Brunswick, NJ) or CDAHFD diet (Research Diets A06071302, New Brunswick, NJ). After 4 weeks on the diet, mice were dosed at 5 mL/kg body weight with vehicle (0.5% methylcellulose and 99.5% water) plus or minus BMS-963272 at 8:00 a.m., once daily by oral gavage for the 8 weeks duration of the study. Body weight was measured weekly in the fed state. EDTA plasma and liver tissue samples were stored at $-80°C$ for later processing. Liver TG levels and plasma ALT, AST, bile acids, NEFA and TG levels were measured on the Olympus AU680 clinical chemistry analyzer (Beckman Coulter, Brea, CA). For histological analyses, liver tissue was fixed in 10% neutral-buffered formalin, processed and sectioned by the Histology Core Laboratory (BMS, Lawrenceville, NJ). Sections of 5 μm were prepared for hematoxylin and eosin (H&E) and picrosirius red staining using a Sakura Tissue Tek Prisma Stainer. For image analysis, all slides were scanned using an Aperio ScanScope (Leica Biosystems Imaging, CA). Analysis was performed on the entire section with HALO platform's (Indica Labs, NM) steatosis quantification or area quantification modules. Individual algorithms were built to detect lipid droplets within the H&E-stained slides, and fibrin within the picrosirius stained slides. Statistical analysis of all the data was performed using one-way ANOVA followed by Dunnett's t test with the CDAHFD vehicle as control using the JMP program from SAS (Cary, NC). All values are mean ± SE. Statistical significance was determined at $p < 0.05$.

Study of BMS-963272 in STAM model of NASH
The efficacy study of BMS-963272 in STAM model was conducted in SMC Laboratories, Tokyo, Japan. NASH was induced in 56 male C57BL/6 mice by a single subcutaneous injection of 200 μg streptozotocin (STZ, Sigma-Aldrich, USA) solution 2 days after birth and feeding them with a high fat diet (HFD, 57 kcal% fat, Ct# HFD32, CLEA Japan, Japan) after 4 weeks of age. Eight NASH mice/group were orally administered either with vehicle (1% methylcellulose) or with BMS-963272 at 0.3 or 3.0 mg/kg in a volume of 10 mL/kg once daily from 6 to 9 weeks of age. The viability, clinical signs and behavior were monitored daily. Body weight was recorded before the treatment. Mice were observed for significant clinical signs of toxicity, moribundity and mortality approximately 60 min after each administration. After the treatment, at age of week 9, mice were sacrificed by exsanguinations through direct cardiac puncture under isoflurane anesthesia (Pfizer) 2 h after the last drug administration. A cohort of 8 NASH mice at 6 weeks of age to serve as a baseline control.

For HE staining, sections were cut from paraffin blocks of liver tissue prefixed in Bouin's solution and stained with Lillie-Mayer's Hematoxylin (Muto Pure Chemicals, Japan) and eosin solution (Wako Pure Chemical Industries). Histological reads were performed in a blinded manner. NAFLD Activity Scire (NAS) was calculated according to the criteria of Kleiner (Kleiner et al., 2005). To visualize collagen deposition, Bouin's fixed liver sections were stained using picrosirius red solution (Waldeck, Germany). For quantitative analysis of fibrosis areas, bright field images of picrosirius re-stained-stained sections were captured around the central vein using a digital camera (DFC295; Leica, Germany) at 200-fold magnification, and the positive areas on 5 fields/section were measured using ImageJ software (National Institution of Health, USA). Plasma samples and frozen liver tissues were sent to BMS for TNFα measurement, BMS-963272 drug exposure and metabolomic studies. Statistical analyses were performed using Bonferroni Multiple Comparison Test on GraphPad Prism 6 (GraphPad Software, USA). p values <0.05 were considered statistically significant. Results were expressed as mean ± SD.

Gut hormone modulation by sub-chronic administration of BMS-963272

HFD (Research Diets, #D12492) acclimated rats were treated with BMS-963272 (30 mg/kg; *b.i.d.*) for 14 days. One hour after the last dose of BMS-963272 or vehicle, *ad libitum* fed animals were sacrificed and plasma was taken for the evaluation of gut hormone levels. The EDTA plasma was prepared by whole blood samples in EDTA supplemented with the DPP4 inhibitor BMS-538305 (3 μM final concentration) and Protease Inhibitor Cocktail (40 μL/mL) and aprotinin. Active GLP-1 levels were measured using an Active GLP-1 ELISA kit (EMD Millipore Corporation; #EGLP-35K). PYY levels were measured using a PYY Fluorescence ELISA kit (Phoenix Pharmaceuticals, # FEK- 059-04). All assays were performed according to the manufacturers' instructions. ANOVA was performed using StatView 5.0.1 (SAS Institute).

Studies on DCA responses after the treatment of BMS-963272 in HFD acclimated rats and mice

Lean C57BL/6J mice were first acclimated to HFD (Research Diets, #D12492) for 10 days. Twenty-four hrs after a single dose of BMS-963272 at 30 mg/kg under high fat diet, plasma samples were taken and stored at −80°C until analyses. Rats were also acclimated to an HFD (Research Diets, #D12492) for 10 days. They were then treated with BMS-963272 at 30 mg/kg (*b.i.d.*) for 7 days while being maintained on HFD. Plasma samples were taken 1 h after the last dose. Plasma samples were protein precipitated in 2 volumes of ice-cold methanol containing 0.1% formic acid and after centrifugation the supernatant was collected and directly injected for liquid chromatography/mass spectrometry (LC/MS) analyses. All DCA measurements were performed by LC/MS on a Thermo Accela-QExactive system. All data was collected at 35K mass resolution with mass accuracy <3 parts per million (ppm) in electrospray full scan negative ion mode. The chromatographic column used was a Waters BEH. The raw mass spectral data was processed with in-house metabolomic software (EDM) and peak area was reported for each individual DCA measured. Statistical analysis was performed in Microsoft Excel using a custom VBA script, which includes calculation of fold-change and P-values using Student's T-TEST analysis.

oLTT study in cynomolgus monkeys

The monkeys were acclimated to HFD (Test Diet 5TNU primate diet, 46.9% of kcal from fat), food deprived overnight, and were then dosed *p.o.* with 1 mg/kg of BMS-963272 or vehicle. They were administered 1 h later by a *p.o.* bolus of Intralipid (7 mL/kg of Intralipid 20%, a 20% soybean oil emulsion). Two weeks after the initial dosing, all monkeys were retested in a within-subject crossover design, allowing each animal to serve as its own control. Plasma TG and DCA levels were measured at various time points.

Diarrhea study in cynomolgus monkeys maintained on HFD

The study consisted of 3 phases, 1) acclimation of monkeys to an HFD, 2) treatment with PF-04620110 and 3) treatment with BMS-963272. For the HFD acclimation phase, monkeys were maintained on the HFD (Purina Lab Diet 5TNU) for 1 month prior to any treatment to establish a baseline for fecal changes. During the second phase, 6 monkeys/sex were dosed orally for 4 days with vehicle and PF-04620110 at 0.1, 0.3 and 1.0 mg/kg/day in an escalating dose regimen with a 1 week washout period between doses. Two additional monkeys/sex received vehicle and served as controls. Approximately 1.5 months after discontinuation of the PF-04620110, BMS-963272 was administered by oral gavage, to monkeys at doses of 1, 10 mg/kg for 4 days in an escalating dose regimen with a 1-week washout period between each dose. Two monkeys/sex received vehicle and served as controls. Abnormal fecal changes were characterized as loose/liquid stool (diarrhea), soft or unformed stool, mucous present, scant feces or absent feces. To estimate systemic exposure of PF-04620110 or BMS-963272, subsequent to the fourth dose of each dose escalation, approximately 200 μL of blood was collected from all monkeys at approximately 1, 2, 4, 6 and 24 h after dosing. Blood samples were collected via the femoral vein in EDTA tubes and PF-04620110 or BMS-963272 concentrations were measured using LC/MS.

Human studies

Clinical study protocol (NCT04116632)

Study title: A Multiple Dose Pharmacokinetic/Pharmacodynamic and Safety and Tolerability Study of BMS-963272 in Obese but Other-wise Healthy Adults.

This was a Phase 1, randomized, double-blind, placebo-controlled, parallel-arm, multiple-dose study designed to investigate the PK and PD effects, and safety and tolerability of multiple dosing regimens of BMS-963272 in healthy adults with obesity. Healthy adult participants age 18 to 60 years, inclusive with a BMI of 30–40 kg/m^2, inclusive were enrolled if they meet all eligibility criteria.

Key inclusion criteria

- Women not of childbearing potential
- Men who are sexually active with women of childbearing potential, including azoospermic men, must agree to follow a highly effective form of birth control as specified in the protocol and refrain from donating sperm.

Key exclusion criteria

- Women who are breastfeeding
- History of relevant medical conditions, including but not limited to Type 1 or Type 2 diabetes, lactose intolerance, gastrointestinal disease or surgery affecting oral absorption, cholecystectomy, malignancy, excessive alcohol consumption per protocol limits
- Clinically significant abnormality in physical examination, vital signs, ECG, or clinical laboratory parameters
- Hemoglobin <10 g/dL (women) or <11 g/dL (men)
- Positive serology for Hepatitis C, Hepatitis B, or HIV
- ALT or AST above the upper normal limits (ULN)
- Total bilirubin > ULN (except if Gilbert's syndrome)
- Estimated Glomerular Filtration rate (eGFR) < 90 mL/min/1.73m2
- TSH >10mIU/L
- Glycated hemoglobin (HbA1c) > 6.5%
- Fasting total cholesterol >300 mg/dL
- Fasting total triglyceride >400 mg/dL
- Systolic blood pressure >150 mmHg and/or diastolic blood pressure >95 mmHg
- Use of weight loss medications within 3 months of screening
- Use of lipid-lowering therapy within 6 weeks of screening

After screening, eligible participants were admitted to a clinical research unit (CRU) on study Day -4 and remained there until discharge on Day 17. They returned for an end-of-study visit on Day 21 ± 3 days.

A total of 36 participants were randomly assigned in an 8 active:4 placebo ratio to 1 of 3 doses groups of BMS-963272: 300 mg once daily (Q24H), 300 mg twice daily (Q12H), or 300 mg three times daily (Q8H), with 12 participants per treatment group.

Primary outcome measures

1. Maximum observed plasma concentration of BMS-963272 (C_{max}) [Time Frame: Day 1, Day 14]
2. Time of maximum observed concentration of BMS-963272 (T_{max}) [Time Frame: Day 1, Day 14]
3. Area under the concentration-time curve in one dosing interval (AUC$_{[TAU]}$) [Time Frame: Day 1, Day 14]
4. Area under the concentration-time curve from time zero to the time of the last quantifiable concentration (AUC$_{0-T}$) [Time Frame: Day 14]
5. Apparent total clearance of the drug from plasma after oral administration (CLss/F) [Time Frame: Day 14]
6. Apparent volume of distribution at steady state (Vss/F) [Time Frame: Day 14]
7. Average concentration at steady state ($C_{avg,ss}$) [Time Frame: Day 14]
8. Half-life (T-HALF) [Time Frame: Day 14]
9. Accumulation index (AI) [Time Frame: Day 14]
10. Rate elimination constant (kel) of BMS-963272 [Time Frame: Day 14]
11. Area under the concentration-time curve (AUC) of triglycerides (TG) and fatty acids in response to the oral lipid tolerance test (oLTT) [Time Frame: Day 7, Day 15]
12. Incremental AUC (iAUC) of TG and fatty acids in response to the oLTT [Time Frame: Day 7, Day 15]

Secondary outcome measures

1. Incidence of Adverse Events (AEs) [Time Frame: Up to 55 days]
2. Incidence of Serious Adverse Events (SAEs) [Time Frame: Up to 55 days]
3. Number of clinically significant changes in vital signs, electrocardiograms (ECGs), physical examinations and clinical laboratory tests [Time Frame: Up to 55 days]

Evaluation of PK parameters

Serial blood and urine sampling at multiple days and times relative to BMS-963272 dosing was performed to assess the pharmacokinetics (PK) of BMS-963272. Individual participant PK parameters were derived from plasma concentration versus time data using noncompartmental methods. Primary plasma PK parameters for BMS 963272 included maximum observed plasma concentration within a dosing interval (C_{max}), time of C_{max} (T_{max}), and area under the plasma concentration-time curve over the dosing interval (AUC$_{[TAU]}$). Secondary plasma PK parameters were area under the concentration-time curve from time of dosing to the time of the last quantifiable concentration observed, average concentration within a dosing interval calculated at steady state (C_{ss}-avg), observed plasma concentration immediately before dose (C_{trough}), terminal elimination phase half-life, apparent total clearance, apparent volume of distribution of terminal phase, degree of fluctuation, AUC accumulation index, and C_{max} accumulation index.

Evaluation of biomarkers in phase 1 study

To assess the PD effects of BMS-963272 in oral Lipid Tolerance test (oLTT) following a standard high fat meal, participants were administered an oLTT meal several times during the study, after which postprandial levels of DCA, gut hormones, TG and FFA were assessed. Blood samples were collected 5 min pre-oLTT and 1, 2, 3, 4, 6, and 8 h post oLTT. The oLTT meal consisted of lactose-free ice cream, lactose-free whole milk, and heavy cream. The test meal was calculated to provide 35 g of fat per square meter of body surface area calculated based on Mosteller formula (Mosteller, 1987) and approximately 60% of calories derived from fat, 30% from carbohydrate, and 4% from protein. All participants had an identical standardized diet at least 24 h prior to the first oLTT and fasted (no food or drink except water) for at least 10 h before each oLTT. After admission to the CRU, participants were administered the oLTT at 1 to 3 days before the start of dosing on Day 1 for a baseline assessment and on Day 15 at 8, 12 and 24 h post last doses for Q8H, Q12H and Q24H, respectively.

All biomarker samples were collected and stored frozen at $-70°C$ before shipping on dry ice to analyzing laboratories. Plasma DCA C18:1 levels were measured using LC/MS method. Plasma samples for total GLP-1 and total PYY were collected in P800 tubes (BD Biosciences) containing a proprietary cocktail of protease inhibitors for stabilization of these peptides. Total GLP-1 and PYY were measured using Meso Scale Discovery (MSD) immunoassay and Linco ELISA assay, respectively, in Nexelis laboratory (Seattle, WA). Bile acids were measured using LC/MS method in the laboratory in Syneos Health (Québec, CANADA).

Safety assessments

Safety assessments were based on medical review of adverse events (AE) reports and the results of clinical laboratory evaluations, 12-lead ECG measurements, vital sign measurements, physical examinations, and the Bristol Stool Consistency Rating to rate each bowel movement.

Statistical methods

A sample size of 12 participants per dose group (8 active:4 placebo) was considered sufficient to achieve the study objectives. Although this number of participants was not based on statistical power considerations, administration of BMS 963272 to 8 participants in each dose group is sufficient to provide approximately 80% probability of observing at least 1 occurrence of any AE that would occur with an approximately 24% incidence in the population from which the sample was drawn.

For DCA 18:1, PYY, and GLP-1 AUC (0-8h), Welch's 2 sample t-tests were used to determine whether the percent change from baseline was significantly different for each treatment group compared to the pooled placebo group. For body weight and waist circumference, a linear mixed model (lmer), which regressed the vital statistic on time, treatment, and time-by-treatment interaction with a random intercept fit for each subject, was used to test whether the change from baseline at day 14 was significantly different for each treatment group relative to the change from baseline of the pooled placebo group. For TCA, TDCA, and FGF21, non-parametric pairwise Mann-Whitney U tests were used to determine whether the percent change from baseline for each treatment group was significantly different from the pooled placebo group. Non-parametric tests were used due to 1 to 2 strong outliers >2 standard deviations above the mean in the placebo groups for each bile acid.

METHOD DETAILS

Mouse plasma TNFα measurement

Mouse plasma TNFα level was measured using Luminex technology with MILLIPLEX MAP Mouse Cytokine/Chemokine Magnetic Bead kit following manufacture instructions (EMD Millipore, catalog no. MCYTOMAG-70K).

RNA-seq study

RNA-seq data from liver and jejunum were harvested from mice fed with CDAHFD diet and methylcellulose vehicle and CDAHFD mice treated with 3 mg/kg of BMS-963272 MGAT2 inhibitor for 8 weeks. RNA-seq libraries were prepared from extracted liver and jejunum RNA independently by using TruSeq Stranded Total RNA Library Prep Gold (Illumina) following the manufacturer's instructions. RNA-seq libraries were sequenced on HiSeq2500 (Illumina) with a target read depth of ~40M per sample. Sequence reads were mapped against the mouse reference genome and gene and transcript abundance was determined by using GRCm38ERCC- ensemble 91 (jejunum) and mm10MTERCC ensemble 80 (liver). Protein coding genes of 14,455 in the jejunum and 14,848 in the liver that passed the low expression filter ($\geq$ 50% of samples with count $\geq$ 10 and median zFPKM $\geq$ −3 [z-transform of fragments per kilobase of exon per million mapped fragments]) were analyzed. Trimmed Mean of M-values (TMM) quality weights (edgeR) to samples followed by limma with voom to assess differential gene expression using a simple model of treatment groups were applied. For pathway enrichment, adjusted p value $\leq$ 0.1 (Benjamini-Hochberg) and an absolute logFC $\geq$ log2(1.15) or log2(1.2) were used to define 1821 genes and 1949 genes differentially regulated by BMS-963272 3 mg/kg in the jejunum and liver, respectively. Pathway enrichment in the meta-baser package was tested for by comparing the relative overlap of regulated genes with pathways to the null hypergeometric distribution.

Apoptotic effect of oleamide on human HSC

Primary human HSCs (ScienCell, catalog no. 5300, Lot 10,744) were plated in 96-well polystyrene cell culture plates at 4,000 cells per well in 100 μL of growth media [DMEM (Gibco, catalog no. 12320), 2% heat inactivated FBS (Sigma, catalog no. F4135),

1x Penicillin-Streptomycin (Gibco, catalog no. 15140)] in 37°C, 5% CO_2 cell incubator. The next day, cells were washed once with 200 µL of PBS, treated with oleamide and other control compounds (all from Sigma) at 1, 10 or 100 µM for 18 h in 100 µL of Assay Media [DMEM (Gibco, catalog no. 11054), 0.1% heat inactivated FBS (Sigma, catalog no. F4135), 1x Penicillin-Streptomycin (Gibco, catalog no. 15140)] in 37°C, 5% CO_2 cell incubator. Cells treated with Assay Media only was used as no apoptosis control (0% Cell death), 2% Triton X-100 made in Assay Media was used as high cell apoptosis control (100% cell death). Cells treated with Caspase inhibitor (Z-VAD-FMK) were included to demonstrate the caspase specificity (Component of CaspACE assay kit, Promega, catalog no. G7220). On the third day, an aliquot of 50 µL of the media was taken out and applied to LDH Cytotoxicity Assay to assess the percent of cell apoptosis following manufacture instructions (Roche Applied Science, catalog no. 11644799001). Caspase 3/7 assays were carried out using kit from Promega, catalog no. G7790.

Metabolomic evaluation of plasma and liver samples from BMS-963272 treated STAM mice

Plasma and liver samples were subjected to protein precipitation by the addition of 3 vol equivalents of methanol solution containing 0.1% formic acid and stable-labeled internal standards in a 96-well plate. The sample plates were mixed in a vortex, centrifuged, split into 2 separate 96-well plates, and dried down to completeness under a nitrogen stream at room temperature. The samples were then reconstituted in the corresponding starting mobile phases, spun down again, 100 uL of each supernatants was transferred into 2 separate 96-well plates, and 10-uL aliquots from each were directly injected for hydrophilic interaction liquid chromatography (HILIC) - and reverse phase (RP)-liquid-chromatography mass spectrometry (LCMS) analyses.

Relative quantitation for each metabolite is determined by integrating the extracted ion chromatograms for the metabolite's characteristic *m/z* and retention time. All LC-MS data were collected using an ultra-high pressure chromatography system interfaced with a Thermo Exactive Plus mass spectrometers. Data analysis for DCAs and fatty amides was performed for the negative reverse phase fraction to determining the peak areas using in-house developed software.

Measurement of small intestinal HETE and EET

Dried small intestinal methanol extracts were reconstituted in 150 µL of 0.1% formic acid:acetonitrile (1:1) containing 500 ng/mL of internal standard (14,15-EET-d1½0-HETE-d6) vortexed to mix then centrifuged. The supernatants (100 µL) were transferred to a shallow 96-well plate and capped for LC/MS/MS analysis. LC/MS/MS was performed on a Sciex (Framingham, MA) API5500 mass spectrometer coupled to a Shimadzu (Kyoto, Japan) Nexera X2 LC-30AD uHPLC pump with Dil-30AC MP autosampler. LC was performed on a Waters (Milford, MA) BEH C18 100 × 2.1 mm 1.7 µm particle size column using a column temperature of 65°C, a mobile phase consisting of solvent A = 0.1% formic acid in water and solvent B = 0.1% formic acid in acetonitrile at a flow rate of 0.6 mL/min. The LC gradient used was as follows: 50-75% B in 2 min, 75-85% B in 2 min, 85-100% B in 2 min, hold 100% B for 1 min. Products were monitored using selected reaction monitoring (SRM) in negative ionization mode. The following ions were monitored: 5-HETE *m/z* 319.2/115.0, 8-HETE *m/z* 319.2/155.0, 11-HETE *m/z* 319.2/167.0, 12-HETE *m/z* 319.2/179.0, 15-HETE *m/z* 319.2/219.0, 5,6-EET *m/z* 319.2/191.2, 20-HETE-d6 (internal standard) *m/z* 325/307.3 and 14,15-EET-d11 (internal standard) *m/z* 330.2/219.2. LC/MS/MS data was acquired using Analyst software. HETE's and EET's were qualitatively determined using the peak area ratio of HETE or EET to the appropriate internal standard. EET and HETE standards were purchased from Cayman Chemical (Ann Arbor, MI).